AEDC-TR-71-91

MAY 11 1971

CURRENT DISTRIBUTION IN CROSSED-FIELD ACCELERATORS (PART IV, PROJECT SUMMARY AND APPLICATION)

G. S. Argyropoulos and S. T. Demetriades

STD Research Corporation

Pasadena, California

April 1971

Approved for public release; distribution unlimited.

ARNOLD ENGINEERING DEVELOPMENT CENTER

AIR FORCE SYSTEMS COMMAND

ARNOLD AIR FORCE STATION, TENNESSEE

PROPERTY OF U S AIR FORCE

F40600-72-C-0002

NOTICES

When U. S. Government drawings specifications, or other data are used for any purpose other than a definitely related Government procurement operation, the Government thereby incurs no responsibility nor any obligation whatsoever, and the fact that the Government may have formulated, furnished, or in any way supplied the said drawings, specifications, or other data, is not to be regarded by implication or otherwise, or in any manner licensing the holder or any other person or corporation, or conveying any rights or permission to manufacture, use, or sell any patented invention that may in any way be related thereto.

Qualified users may obtain copies of this report from the Defense Documentation Center.

References to named commercial products in this report are not to be considered in any sense as an endorsement of the product by the United States Air Force or the Government.

CURRENT DISTRIBUTION IN CROSSED-FIELD ACCELERATORS (PART IV, PROJECT SUMMARY AND APPLICATION)

G. S. Argyropoulos and S. T. Demetriades
STD Research Corportation
Pasadena, California

Approved for public release; distribution unlimited.

FOREWORD

The work reported herein was sponsored by Arnold Engineering Development Center (AEDC), Air Force Systems Command (AFSC), Arnold Air Force Station, Tennessee, under Program Element 62201F, Project 8950, Task 895012.

The research was performed by STD Research Corporation, Box 4127, Catalina Station, Pasadena, California, under Contract F40600-70-C-0001. The work reported herein was performed from 1 July 1969 to 30 September 1970. Technical monitor was Lieutenant Thomas G. Horn.

The reproducibles used in the reproduction of this report were supplied by the authors.

This technical report has been reviewed and is approved.

Thomas G. Horn
First Lieutenant, USAF
Research and Development Division
Directorate of Technology

Harry L. Maynard
Colonel, USAF
Director of Technology

ABSTRACT

Realistic analytical modeling of crossed-field accelerators is obtained by computing the development of turbulent magnetohydrodynamic boundary layers on the walls and the coupled two-dimensional distributions of current density, plasma properties, and fluid velocity, temperature and pressure over the entire channel. The analysis is based on methods developed in previous work by the authors, and considers the effects of electron nonequilibrium, thermal and concentration diffusion, suppression of turbulence by magnetic fields, finite reaction rates, and electron energy relaxation. Application to the Hirho channel gives excellent agreement with experimental results. It is shown that the reduction of the Hall field in Faraday channels is due to the fact that local axial current density is present over most of the flow, even when there is no net current leakage along the channel. The modeling is carried out by a well-documented computer program, of which a program listing, Fortran source deck, and explanation of input and output formats are provided. This work has demonstrated that realistic computations are necessary for the design of efficient magnetohydrodynamic channels.

TABLE OF CONTENTS

LIST OF FIGURES

NOMENCLATURE

General Notation

$A^{(2)}$, $A^{(5)}$	Weighting factors in the computation of the coefficients of Ohm's law
a_1, a_2, a_3	Universal turbulence structure parameters
$\vec{B}$	Magnetic field vector
c_α	Partial mass concentration of component α in the plasma
c_f	Wall skin friction coefficient
c_p	Specific heat at constant pressure
c_v	Specific heat at constant volume
D	Channel dimension in y-direction
$\vec{E}$	Electric field vector
H	Total enthalpy per unit mass, $h + u^2/2$
H	Shape factor, δ^*/θ (Appendix A only)
h	Specific enthalpy, $\int_0^T c_p \, dT$
$\vec{J}$	Electric current density vector
$\vec{J}_h$	Heat flux
$\vec{K}$	Thermal diffusion vector
$\vec{k}$	Unit vector in z-direction
k	Boltzmann's constant
k_f	Forward reaction rate constant
k_r	Reverse reaction rate constant
L	Electrode period, in a multielectrode geometry
L_c	Length of conductor segment, in a multielectrode geometry
L_E	Electron energy relaxation length
L_R	Ionization relaxation length
M	Mach number
$\dot{m}_E$	Mass entrainment rate at outer edge of the boundary layer
$\dot{m}_I$	Mass flux through the inner edge of the boundary layer
N	Number of plasma components
n_α	Number density of each component α
p	Gas pressure

Q	Collision cross section for momentum transfer
Re_θ	Momentum thickness Reynolds number, $U_\infty \theta/\nu$
S	Mass flow stream function
St	Stanton number
T	Gas temperature
T_a	Characteristic temperature of each component a
$\vec{U}$	Mass average velocity vector
U_∞	Velocity outside the boundary layer
u	x-component of $\vec{U}$
v	y-component of $\vec{U}$
x	Streamwise coordinate
y	Coordinate across electrodes, normal to x
z	Coordinate along the magnetic field direction
β	Hall coefficient in Ohm's law
δ	Thickness of boundary layer
δ_{995}	Value of y where $u(y) = 0.995\ U_\infty$
δ^*	Displacement thickness (see Appendix C)
ϵ	Ohm's law coefficient
θ	Momentum thickness (see Appendix C)
ν	Kinematic viscosity
ρ	Mass density
σ	Scalar electrical conductivity
τ	Turbulent sheer stress
τ_L	Laminar sheer stress
φ	Angle between current vector and y-axis
Φ	Electrical potential
Ψ	Electric current stream function
ω	Normalized transverse coordinate in boundary layer

Subscript Notation

CL	Centerline
E	Evaluated at the outer edge of the boundary layer
e	Pertaining to electrons

I	Evaluated at the inner edge of the boundary layer
i	Pertaining to ions
L	Denotes laminar contribution
T	Denotes turbulent contribution
w	Evaluated at the wall
α	Pertaining to any plasma component
1, 2, 3	Vector component along x-, y-, and z-directions, respectively
∞	Pertaining to conditions outside the boundary layer

I. INTRODUCTION

The design of efficient and long-lived magnetohydrodynamic channels requires the exactness of a sufficiently realistic, powerful and reliable theory for modeling and predicting the performance. The lack of such a theory up to now has been one of the main reasons for the lack of convincing success and progress in this field. The MHD problem is so complex, and the performance of crossed-field devices depends on so many interrelated variables and physical mechanisms, that one cannot rely on the Edisonian approach of experimental development nor hope for a von Karman type simplification. In fact, realistic description of the overall performance characteristics of magnetohydrodynamic channels can be obtained only by accurate knowledge of the local behavior at every point in the channel, and rigorous analytical account of the physical mechanisms that influence the flowing plasma.

Such a realistic analytical method for modeling and predicting the performance of crossed-field accelerators has been developed by STD Research Corporation under the sponsorship of Arnold Engineering Development Center through Contract AF 40(600)-1166. During the three phases of this completed work (Refs. 1, 2), a rigorous two-dimensional theoretical model for the coupled electrical and gasdynamic behavior over any prescribed accelerator length has been formulated, and numerical solution of this model has been obtained. The formulation of the model is very general and permits detailed analysis of the effects of electron nonequilibrium, thermal and concentration diffusion, electrode-wall boundary layers, finite reaction rates, and electron energy convection on accelerator performance. The numerical solution employs very powerful and fast methods (e.g., an extremely efficient direct method of solving the elliptic streamfunction equation in two dimensions), with the only exception that, in the core of the flow, the solution of the gasdynamic part of the problem has been limited up to a quasi-one-dimensional rather than fully two-dimensional method.

The purpose of the work reported herein, which followed the three phases of Contract AF 40(600)-1166, was not to extend the above realistic

analytical model, but rather to simplify it, test it, and apply it to accelerator designs of current interest to AEDC; also, to document the computer program by which the modeling is performed.

The applications show that, unlike previous idealized or over-simplified theories, this method can predict experimental results, like the distribution of Hall potential, with impressive accuracy, and it provides truly realistic analytical modeling of magnetohydrodynamic channels.

They also show that, to attain equal accuracy in describing the asymmetries between the turbulent boundary layer profiles on the anode compared to the cathode wall of magnetohydrodynamic channels, the numerical solution must be extended to employ fully two-dimensional methods for the gasdynamic part of the problem in the core of the flow. This last remaining extension of the present analytical model can be accomplished with modest additional effort.

The groundwork for this realistic analytical modeling has been the formulation of a simple and accurate Ohm's law in multicomponent nonisothermal plasmas (Ref. 3) followed by experimental measurement of electron-neutral collision cross sections for momentum transfer (Ref. 4), the precise definition and experimental measurement of electron-neutral energy loss factors (Refs. 5 and 6), the derivation of criteria for the relaxation effects (Ref. 7), and a novel formulation of the problem of compressible, turbulent, magnetohydrodynamic boundary layers (Ref. 8), Very helpful also was the early work on the classification of MGD flows (Ref. 9), as well as the recent tabulation of electron-neutral collision cross sections and associated weighting functions in various gases (Ref. 10).

Thus, making use of the MGD flow classification scheme and definitions of Demetriades (Ref. 9), the authors can now claim to have solved the ($U_{1,2}$, B_3, $E_{1,2}$) - dimensional compressible turbulent coupled MGD problem in the boundary layers and the (U_1, B_3, $E_{1,2}$) - dimensional compressible problem in the core of the flow.

II. THE ANALYTICAL MODEL

Description of the detailed local behavior at every point in the channel is obtained by solving for the coupled distributions of both the electrical and gasdynamic fields over any prescribed accelerator length. The electrical part involves the distributions of current density $\vec{J}$, electric field $\vec{E}$, and of the plasma transport properties (conductivity σ, Hall parameter β, ion-slip parameter ϵ, etc.). The gasdynamic part involves the distributions of fluid velocity $\vec{U}$, temperature T, pressure (or density) p (or ρ), and turbulent shear stress τ, including profile developments for velocity, temperature, and shear stress in the electrode-wall boundary layers.

Fig. 1 is a schematic diagram of the analytical problem that has been solved in this study. Two independent variables are considered: x in the direction of the overall plasma flow and y in the direction of the applied electric field. The magnetic induction $\vec{B}$ is assumed to be directed in the positive z-direction and to be a known function of x. Three classes of two-dimensional fields are computed as unknowns: First, the electrical unknowns, namely the current density field $\vec{J}$ and the electric field $\vec{E}$ at every point in the gas. Second, the unknowns that characterize the state of the plasma, namely the number density n_a of each component a that is needed for this purpose, and its characteristic temperature T_a. (Plasma transport properties are then calculable by the methods of Ref. 3.). Finally, the gasdynamic fields, namely the gas density ρ or pressure p, gas velocity $\vec{U}$, static gas temperature T, and shear stress τ. If values for the gasdynamic distributions are assumed, and the first two classes of unknowns (which are coupled) are solved for, this is called solution of the (still nonlinear) "electrical part" of the problem (see Fig. 1). If values for the current density or the electric field distribution are assumed, and the last two classes of unknowns are solved for, this is called solution of the "gasdynamic part" of the problem (see Fig. 1). These partial problems were solved in Phases I-III of Contract AF 40(600)-1166. Then, these partial solutions were used to obtain the solution of the complete, coupled "electrical + gasdynamic" problem over any prescribed channel length, by iteration between the electrical and gasdynamic parts of the problem. Note that the solution

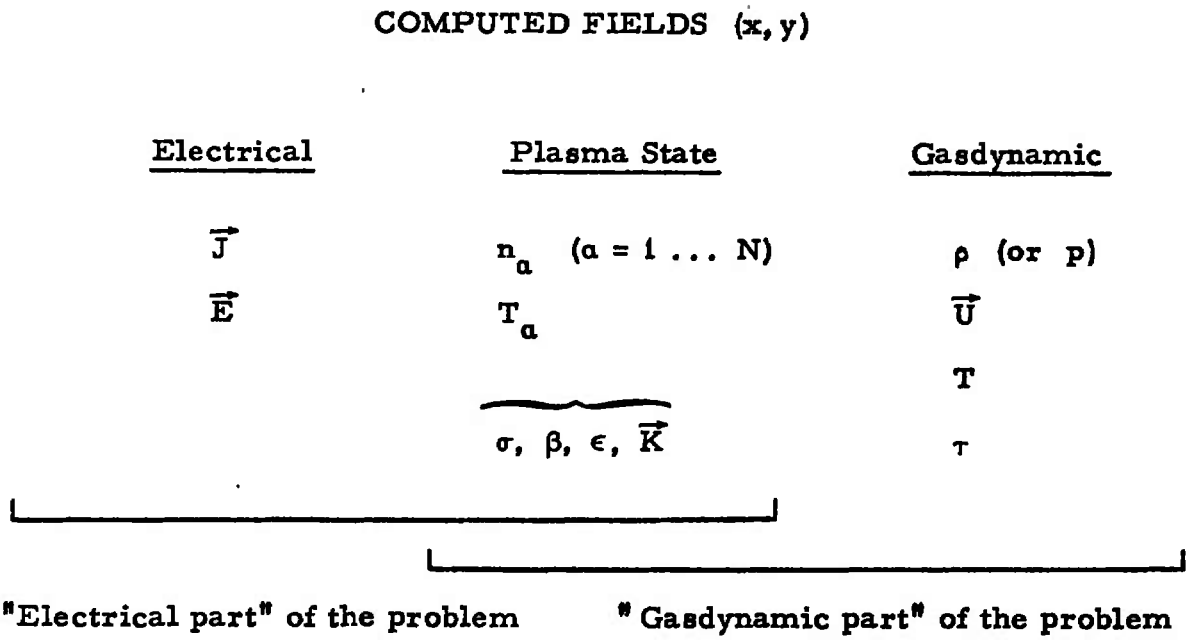

Fig. 1. Schematic diagram of the analytical problem solved in this study.

of the gasdynamic part of the problem includes computation of the compressible turbulent magnetohydrodynamic boundary layer development, for which a novel formulation (Ref. 8) has been used; its accuracy has been checked by application to test cases for which experimental results are available, and the excellent results are described in Appendix A. (For further details see Ref. 2.)

The aforementioned iteration between the electrical and gasdynamic parts of the problem to obtain the solution to the coupled problem is carried out as follows:

(1) Start by using a given distribution of plasma transport properties and thermal diffusion vector $\vec{K}$. (For example, at the outset of a computation, uniform (constant) properties and $\vec{K} = 0$ are usually assumed.)

(2) Then solve the streamfunction equation (see Refs. 1, 2) to obtain the current streamfunction Ψ.

(3) Differentiate Ψ numerically to obtain the components of the current density vector $\vec{J}$.

(4) Then solve the gasdynamic part of the problem first in the core and then in the electrode-wall boundary layers. This gives a new distribution of the variables that determine the plasma properties, i.e., of the gas temperature T, the electron temperature T_e and the number densities n_a ($a = 1...N$) of all the plasma components that are needed to characterize the state of the plasma.

(5) Finally, calculate, at each point of the numerical grid, the corresponding plasma transport properties by the methods of the authors' basic work on Ohm's law (Ref. 3).

At this point one cycle of the iteration has been completed, and further cycles are obtained by starting again with Step (2).

The iteration described above has been found to converge rapidly. Specifically, approximately four cycles were sufficient for convergence in the case of the Hirho channel.

Appendix B describes the computer program COUPLED that has been coded in FORTRAN to carry out the numerical solution of this analytical model. It includes a list of routines and important variables, specification of required input data and formats, and a description of available output.

To provide the experimentalist and development engineer with truly rigorous and practical assistance in the design of crossed-field accelerators, every effort has been made to maintain maximum flexibility in the analytical modeling. Thus, the computer program can treat (1) different channel, electrode, and insulator geometries, including "staggered" electrodes, (2) different operating modes and magnetic field distributions, (3) different current leakage rates, (4) different combinations of boundary layer and core flow initial conditions, (5) different operating fluids (monatomic, diatomic, or mixtures of gases), (6) different seed materials and seed ratios, (7) different electrode and wall temperatures and cooling rates, (8) different wall ablation rates, and (9) different load conditions.

III. APPLICATIONS AND CONCLUSIONS

The realistic analytical model described in the previous Section was used to predict and analyze the performance characteristics of the Hirho accelerator at Arnold Engineering Development Center.

The results and conclusions are discussed in this Section. Particular attention was given (a) to the determination of the specific physical mechanisms leading to the differences in Hall potential as calculated by one-dimensional theory and as calculated by the complete theory used here, and (b) to the development of the turbulent boundary layer profiles on the electrode walls, and to possible asymmetries between these profiles on the anode and cathode wall.

1. HALL POTENTIAL VARIATION

The axial electric field E_x, or equivalently, the axial variation of the electric potential Φ, is an important parameter in characterizing the overall performance of magnetohydrodynamic channels.

It is well known that previous theories have failed — by as much as an order of magnitude — in predicting and interpreting experimental measurements of the Hall potential. Very convincing in this respect are the examples presented by W. Norman and L. G. Siler for the computed vs. measured Hall potential in the Hirho channel at Arnold Engineering Development Center (Ref. 11, Figs. 29a-29h). When they say "computed," Norman and Siler mean the results of their quasi-one-dimensional method of solution, and their Figures 29a-29h plot the variation of the cathode potentials along the channel and thus provide comparison of the computed results with directly measured experimental data. Fig. 2 of this report reproduces one of the cases reported in Ref. 11 (specifically Run 1412), but also includes the results computed in this study concerning the potentials of the first eight cathodes relative to cathode #1. The agreement of the results computed in this study with the experimental measurements is remarkable. This is particularly so in view of the very different results given for the same case by the computer program of Ref. 11, which prompted the authors to emphasize the great difference between "theory" and experi-

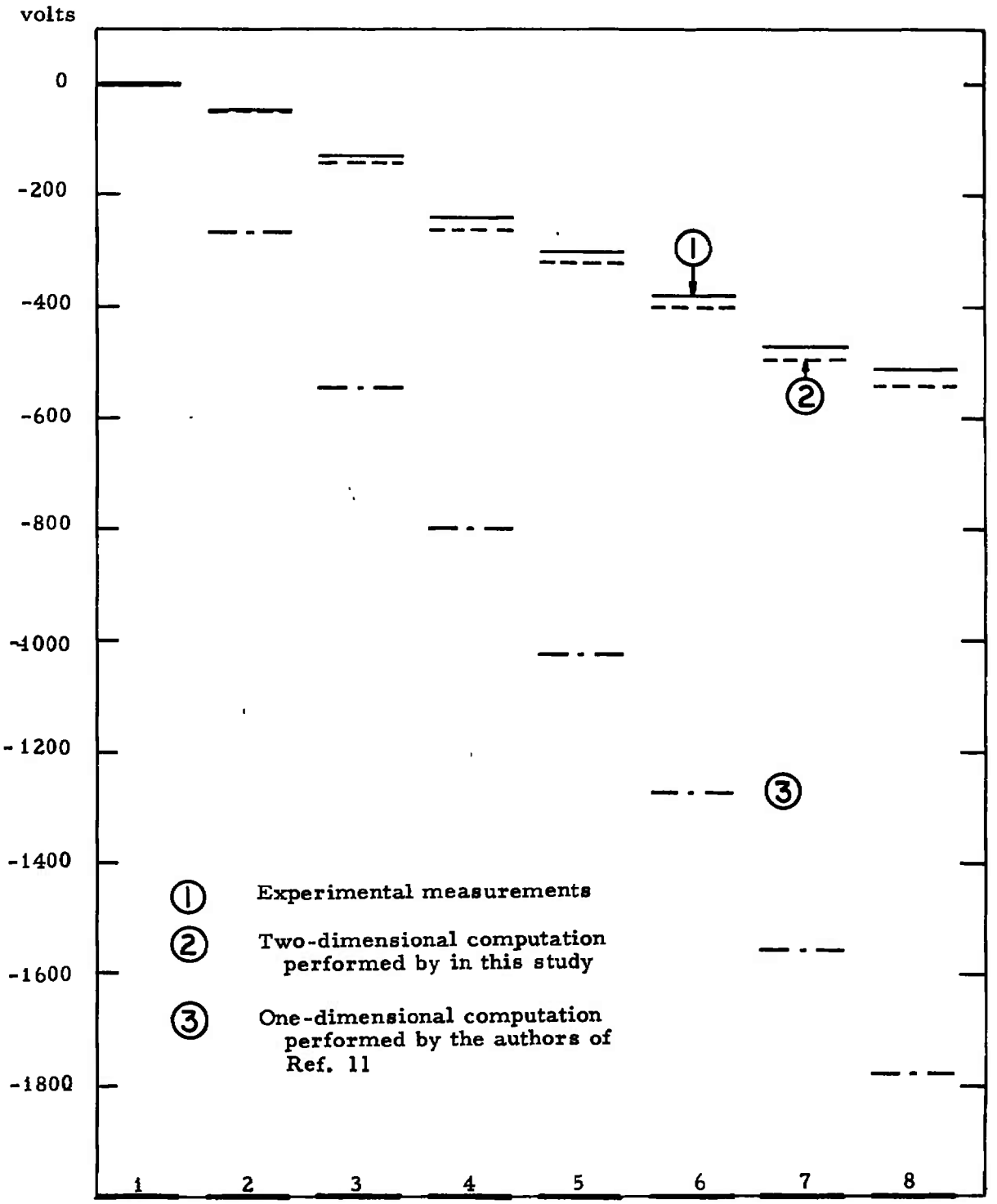

Fig. 2. Cathode potentials in the Hirho channel, referenced to cathode #1 [operating conditions of Run 1412 (Ref. 11)]

ment. The following will analyze briefly how the methods used in this study give this better agreement with experiment by accounting properly for all the physical mechanisms that influence the Hall potential variation in MHD channels.

Let us consider the variation of the electric potential Φ on the centerline of a channel (which is the quantity that one-dimensional methods can compute). Since, by definition

$$\vec{E} = -\nabla\Phi \quad , \tag{1}$$

the Hall potential on the centerline can be defined as

$$\Phi_{CL}(x) = -\int_o^x \vec{E} \cdot d\vec{\ell} = -\int_o^x E_x \, dx \tag{2}$$

The Hall field E_x at any point in the channel is related to the current density components J_x and J_y in terms of Ohm's law (Refs. 3 and 4)

$$\vec{E} + \vec{U} \times \vec{B} + \vec{K} = (\epsilon/\sigma)\vec{J} + (\beta/\sigma)\vec{J} \times \vec{k} \tag{3}$$

where $\vec{K}$ is the thermal diffusion vector, $\vec{k}$ the unit vector in the z-direction, $\vec{B} = B\vec{k}$ the magnetic induction, $\vec{U}$ the plasma velocity, σ the scalar conductivity, β the Hall coefficient, and $\epsilon \approx 1$ a coefficient associated with ion slip. (See Ref. 2 for detailed definitions of parameters and geometry.) Ohm's law can be written in the x-direction in the form

$$E_x + K_x = \frac{1}{\sigma}[\epsilon J_x + \beta J_y]$$

$$= \frac{\epsilon}{\sigma} J_y [-\mathrm{tg}\varphi + \frac{\beta}{\epsilon}] \tag{4}$$

where φ is the signed angle between the y-axis and the current density vector $\vec{J}$. [According to this definition of φ, it is clear that

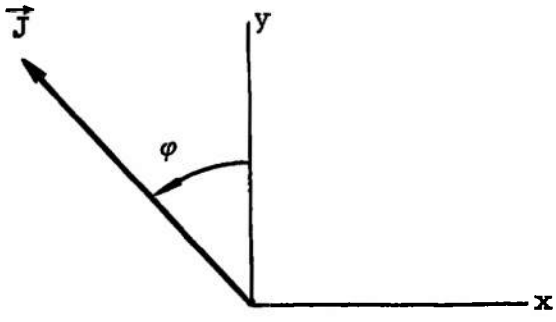

$$J_x = -J_y \mathrm{tg}\,\varphi \tag{5}$$

In a crossed field accelerator J_y is positive. A positive value for φ thus

implies negative value for J_x, as in the figure.] On the centerline of crossed-field accelerators, where x-gradients of plasma properties are small, K_x will be generally negligible compared to E_x.

It is clear from Eq. (4) that in a crossed-field accelerator, for which the average current density J_y is known from the loading conditions, the Hall field E_x (and hence the Hall potential Φ_{CL}) is influenced by three factors, namely

(1) the current distribution (more precisely, the slope φ of the current lines),
(2) the value of the Hall coefficient β/ϵ, and
(3) the value of the scalar conductivity σ.

The last two of the above factors concern transport properties of the gas that can be readily computed (Ref. 3) once the plasma composition and the electron temperature T_e are known. The latter is of course a function of the Ohmic heating of the gas, and is computed via the electron energy equation (Ref. 2). In general, the Hall coefficient β/ϵ has a negative variation with T_e, namely

$$\frac{d}{dT_e}(\beta/\epsilon) < 0 \tag{6}$$

while the scalar conductivity σ usually has a strong positive variation with T_e, namely

$$\frac{d}{dT_e}\sigma > 0 \tag{7}$$

In other words, a higher value of the electron temperature T_e would lead to lower value for β/ϵ and higher value for σ. A glance at Eq. (4) shows that both of these effects would tend to lower the Hall field E_x. Consequently, one could replace factors (2) and (3) of the previous paragraph by considering simply the level of the electron temperature on the centerline of the channel.

It is now clear that the presence of a finite, negative J_x in the core of the flow tends to lower the Hall field E_x, and the Hall potential Φ_{CL} in crossed-field accelerators because of two factors. First, it leads to a positive value of tg φ, which enters with a negative sign in Eq. (4). Secondly, it leads to increased local Ohmic heating

$$(\vec{E} + \vec{U} \times \vec{B}) \cdot \vec{J} \approx \frac{\epsilon}{\sigma} (J_x^2 + J_y^2)$$

$$= \frac{\epsilon}{\sigma} J_y^2 \frac{1}{\cos^2 \varphi} \tag{8}$$

Increased Ohmic heating leads in turn to higher gas temperature T and electron temperature T_e, which implies, according to the previous paragraph, lower E_x because of lower β/ϵ and higher σ. The separate contribution of each one of the above two factors has been analyzed in Ref. 2, where it was shown that both are important.

It is concluded that the Hall potential in crossed-field accelerators is influenced directly and strongly by the two-dimensional current distribution in the channel. As shown in the authors' previous work, the current distribution is dependent upon many nonlinear physical mechanisms (including non-uniformities, thermal and velocity boundary layers, finite reaction rates, electron energy relaxation) and that all of these mechanisms must be accounted for, before the current distribution can be computed with any degree of confidence. This has been the purpose and the accomplishment of the work performed in Phases I-III of Contract AF 40(600)-1166. In contrast, one-dimensional computations have no means for even estimating the current distribution; they just rely on assumed values for J_x and J_y. (Note, of course, that the average value of J_y on the centerline can be estimated fairly reliably in a multielectrode channel from the total current that is passed between the electrodes. But no such estimate is available for J_x, which cannot be found by anything short of a two-dimensional computation.)

This inability to estimate J_x is thus the reason why quasi-one-dimensional computations have consistently failed to provide meaningful

results for the Hall potential in crossed-field accelerators. They can do so only if, somehow, they manage to estimate J_x correctly under the given operating conditions. But, in view of the complicated effects analyzed in Refs. 1, 2, to reach such a correct estimate would be a miraculous coincidence. Let us note, in addition, that many one-dimensional computations forget to account for the increased Ohmic heating because of the presence of J_x.

The two-dimensional current distribution over the region of the first seven electrode-pairs of the Hirho channel (including entrance effects), as computed by the methods of this study, is shown on Fig. 3(b).

After the effect of finite J_x was demonstrated, additional computations were performed by these methods to investigate possibilities of improving the performance by diminishing the angle φ through changes in the electrode geometry. Thus, a computer run treated a "staggered-electrode" geometry, where the cathodes were shifted in the downstream direction by 5/9 of the electrode of period (i.e., approximately 1") compared to the position of the corresponding anodes. Finally, a third run treated a geometry with much shorter conductor segments (L_c reduced by a factor of 3) but unchanged insulator segments — which resulted, of course, in finer electrode segmentation (L/D = 5/9 instead of 9/8). The operating conditions used in all computations were those of Run No. 1412 (Ref. 11). The results are shown on Figs. 3 and 4.

Figure 3 (a) shows the current distribution in the actual Hirho geometry as computed by the idealized "constant property" method, to contrast with Fig. 3(b) which shows the current distribution as computed by the present method, including thermal diffusion, finite reaction rates, and electron energy convection. The generally greater angle φ between the current lines and the y-axis (and correspondingly greater J_x for given J_y) is the most noticeable characteristic of Fig. 3(b) as compared to Fig. 3(a). The potential distribution corresponding to the current distribution of Fig. 3(b) is shown on Fig. 3(c), on which the contours are equipotentials for the electric field $\vec{E}$ (unprimed) and the contour interval is 50 volts.

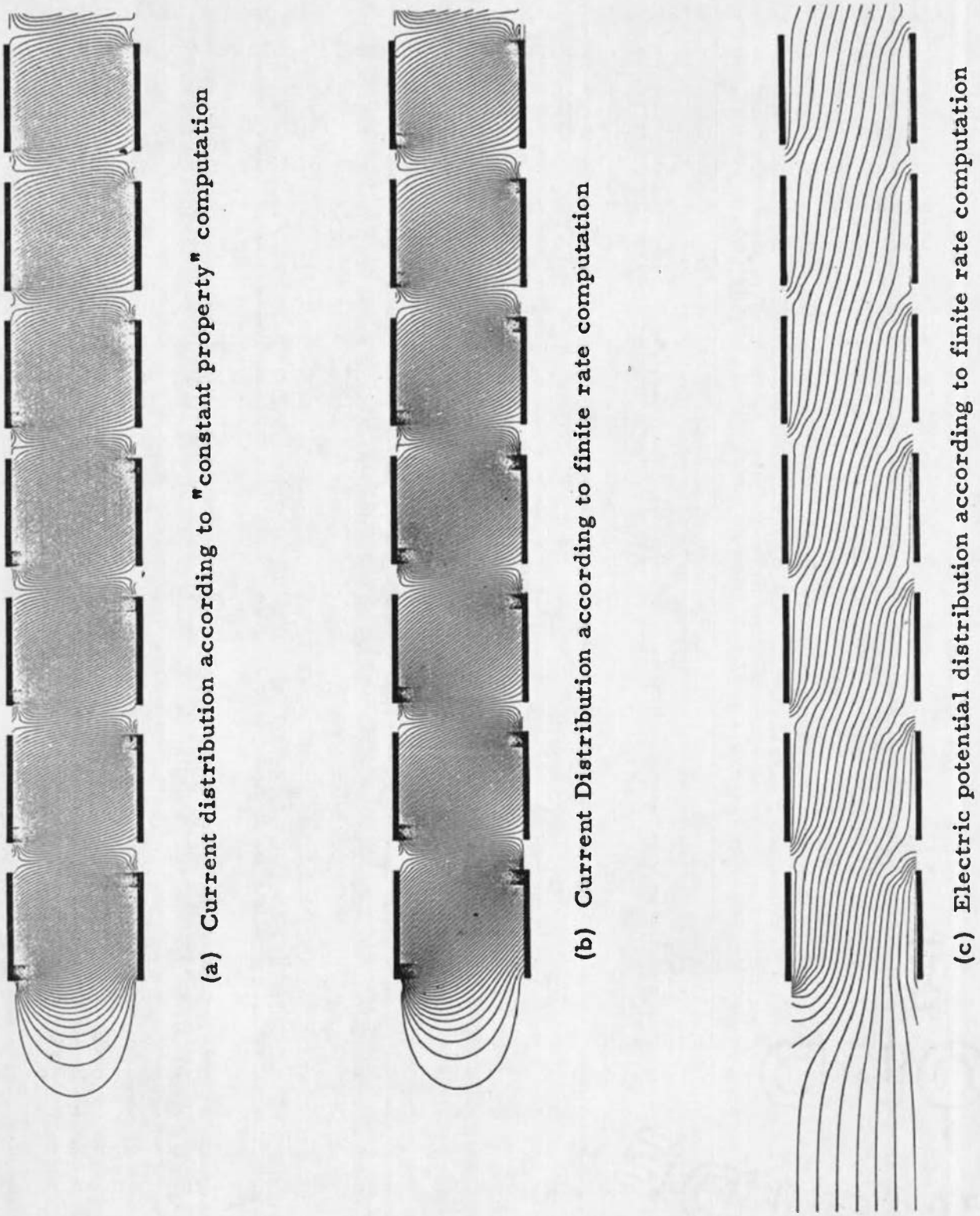

Fig. 3. Current and electric potential distributions for actual Hirho geometry.

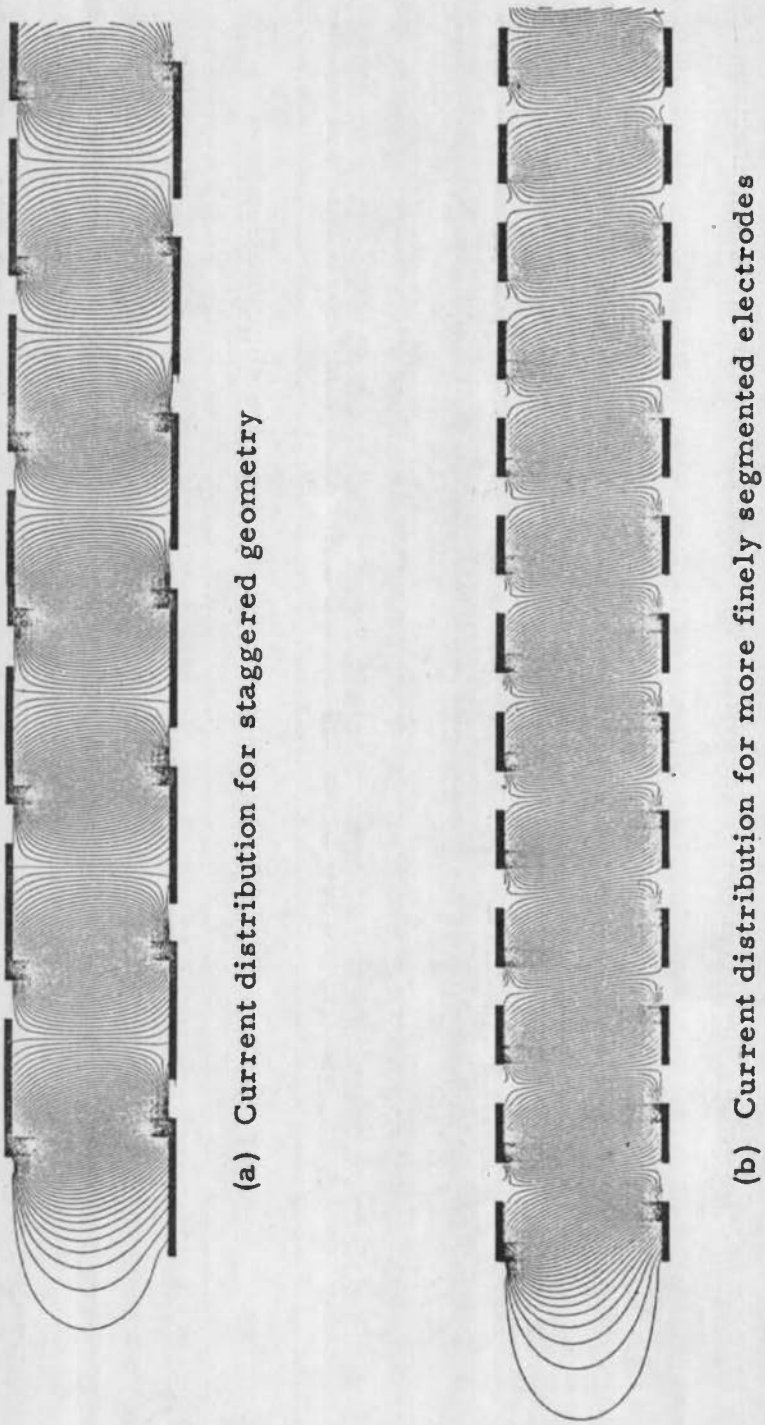

Fig. 4. Current distributions corresponding to modified Hirho geometries.

The importance of optimum electrode configuration for the performance of MHD devices has been often pointed out by the authors (Refs. 1, 12, 13) and is clearly illustrated by Figures 4(a) and 4(b). Figure 4(a) shows the current distribution in the "staggered-electrode" geometry, and demonstrates that in this case the angle φ has an average value of the order of 5° as opposed to 20° in the actual geometry (Fig. 3(b)). Finally, Fig. 4(b) shows the current distribution in the case of shorter conductor segments for which the average value of the angle φ is of the order of 10°, and demonstrates the efficiency of achieving finer segmentation by shorter conductor segments alone (Ref. 12).

2. TURBULENT BOUNDARY LAYER DEVELOPMENT

The development of turbulent boundary layers on the walls of MHD channels is a very decisive factor of the observed overall performance, since it determines the pressure distribution along the channel and the possibility of channel "choking" or stalling. For example, it has been reported for the Hirho channel (Ref. 11) that only 50% -80% of the theoretically predicted pressure drop was realized in actuality. This is the reason that special attention was given to the boundary layer problem in this study, leading to the formulation of a powerful new analytical treatment of compressible, magnetohydrodynamic, turbulent boundary layers (Refs. 2 and 3). This treatment takes into consideration the influence of fluctuating electromagnetic fields on the mechanisms of turbulence, illustrated for example by the well-known phenomenon of turbulence suppression in magnetic fields. Test cases, for which experimental results are available, have established the accuracy of this new formulation (see Appendix A).

Application of these methods, and solution of the coupled problem, has yielded the two-dimensional boundary layer development in the Hirho channel under the operating conditions of Run No. 1412 (Ref. 11).

The reader is reminded that the working fluid was air seeded with 0.2% (by weight) potassium. The geometry and operating conditions were those for which the electrical and, separately, the gasdynamic problem had been solved previously (Ref. 2). Thus the computation started (x=0) at a point 6.8 cm (~3") upstream of the first electrode — which is 33.8 cm

(~ 13-1/2") downstream of the throat — and ended ($x = x_F$) at the end of the fourth electrode pair, 23.8 cm (9-1/2") later — i.e., ~ 23" from the throat (see Ref. 11). It should be noted that the separate solution of the gas dynamic problem had previously been carried out to the end of the tenth electrode pair; the coupled solution reported here, however, was carried out only up to the end of the fourth electrode pair because of computer storage limitations. It is of course a simple matter to continue the computation further, to the end of the tenth electrode or beyond.

The flow conditions at the selected initial station $x = 0$ were as follows, where the subscript ∞ means $y = \delta$ (free stream) and the subscript w means $y = 0$ (wall):

$$U_\infty = 2850 \text{ m/s}$$

$$T_\infty = 3180 \ ^\circ\text{K}$$

$$T_w = 300 \ ^\circ\text{K}$$

$$p = 5.73 \text{ atm}$$

$$dp/dx = 3.3 \text{ N/m}^3$$

$$\delta_{anode} = \delta_{cathode} = 6.1 \text{ mm}$$

The initial profiles of the gas velocity u and the gas temperature T — i.e., the functions $u(0,y)$ and $T(0,y)$ — were taken to be symmetric on the anode and cathode walls and were computed on the basis of a 1/7th power law variation of the ratios u/U_∞ and $(T-T_w)/(T_\infty - T_w)$ with respect to y/δ.

The magnetic induction B was taken to vary in the flow direction from the value 2.52 Wb/m^2 at $x = 0$ to the value 2.82 Wb/m^2 at $x = x_F$ (Refs. 2 and 11).

The axial variations of U_∞ and of the current density components J_x and J_y on the anode and cathode walls were obtained simultaneously by the coupled solution described in Section II.

The solution has provided, in addition to the description of the boundary layer development, the distributions of skin friction and wall heat transfer rate along the channel. The results are shown on Figs. 5-11.

Figures 5, 6, 7, 8, and 9 present the profiles of the unknowns u, τ, T, n_e, and T_e, respectively, at the initial station $x = 0$, and at three subsequent x-stations. As has already been mentioned, the initial profiles are all assumed to be symmetric with respect to the centerline, i.e., that there is no difference between the anode and cathode wall at $x = 0$. The development of these profiles, and the appearance of asymmetries at downstream stations, is shown clearly by these figures. The development of the velocity profile, as shown on Fig. 5, demonstrates an almost symmetric flattening, as the boundary layers start growing to almost fill the channel at the end of the geometrical region of interest. The acceleration achieved in the core of the flow is illustrated clearly. Figure 6 shows the development of the turbulent shear stress profile. At the initial station, $\tau(0, y)$ is computed from the assumed velocity profile through use of a mixing length expression. The subsequent profiles are computed by the present method through solution of a transport equation for τ (Ref. 2). Note that if the laminar contribution τ_L were added to τ, and the total shear stress $\tau_L + \tau$ were plotted, it would have a maximum at the wall due to the effective favorable pressure gradient in the supersonic diverging channel. Figure 6 indicates that the τ-profile develops, like the u-profile, in an almost symmetric way on the anode and the cathode wall. This apparent symmetry would be affected if three-dimensional effects had been taken into consideration. Figure 7 shows the development of the mean gas temperature profile. It also was assumed initially to be symmetric, according to the 1/7 power law, but Fig. 7 shows that this assumed initial profile is soon affected strongly by Ohmic heating and dissipation so as to develop asymmetric peaks close to the anode and

cathode walls at downstream stations. This nonuniformity would have been more pronounced if the geometry had extended axially to the end of the entire MHD section. Definite asymmetries also appear in the downstream development of the n_e and T_e profiles, shown on Figures 8 and 9, respectively. In obtaining these profiles, the restriction of uniform core was relaxed.

The computed results for the variation of the skin friction coefficient c_f and the heat transfer coefficient St along the channel are shown on Fig. 10. The asymmetry between anode and cathode walls is relatively small. The skin friction results lie between those obtained by the method of Enkenhus and Mahez and by that of Elliot, Bartz, and Silver and reported in Ref. 11. Finally, the computed growth of the boundary layer thickness δ and of the displacement thickness δ^* are shown on Fig. 11. Again the asymmetry is relatively small. The displacement thickness, by definition, reduces the effective channel height D for the core flow. Taking into consideration that the channel height D at the initial station $x = 0$ is 3.1 cm, and the angle of divergence of the channel is $1^\circ 26'$, we see that the ratio δ^*/D varies from approximately 2.5×10^{-2} at $x = 0$ to 3×10^{-2} at $x = 24$ cm.

Definitions of the characteristic quantities of turbulent boundary layers that are used in this study are given in Appendix C.

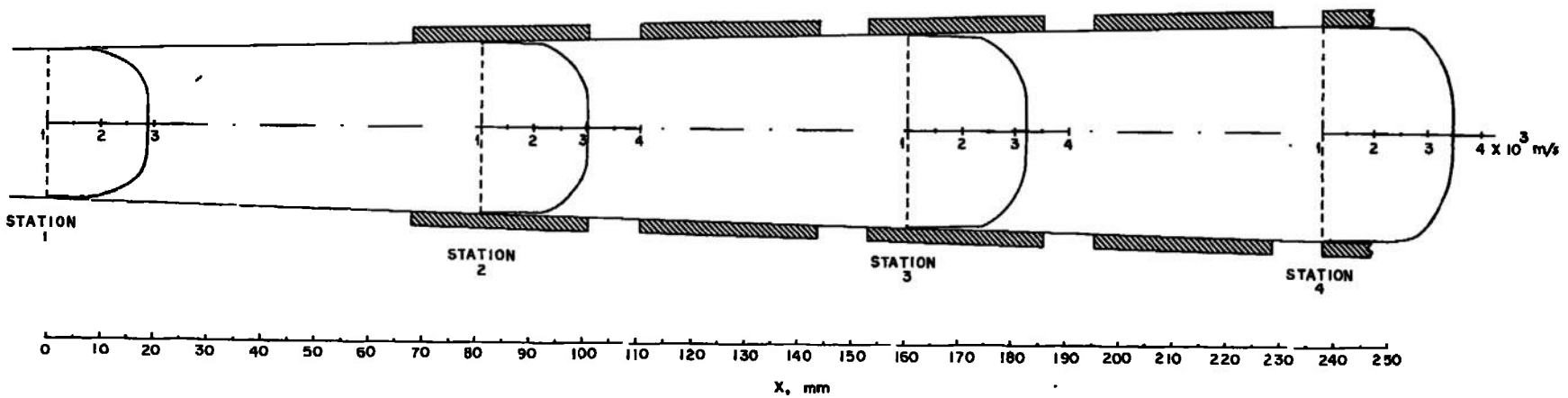

Fig. 5. Development of mean velocity profile in the Hirho accelerator [operating conditions of Run 1412 (Ref. 11)]

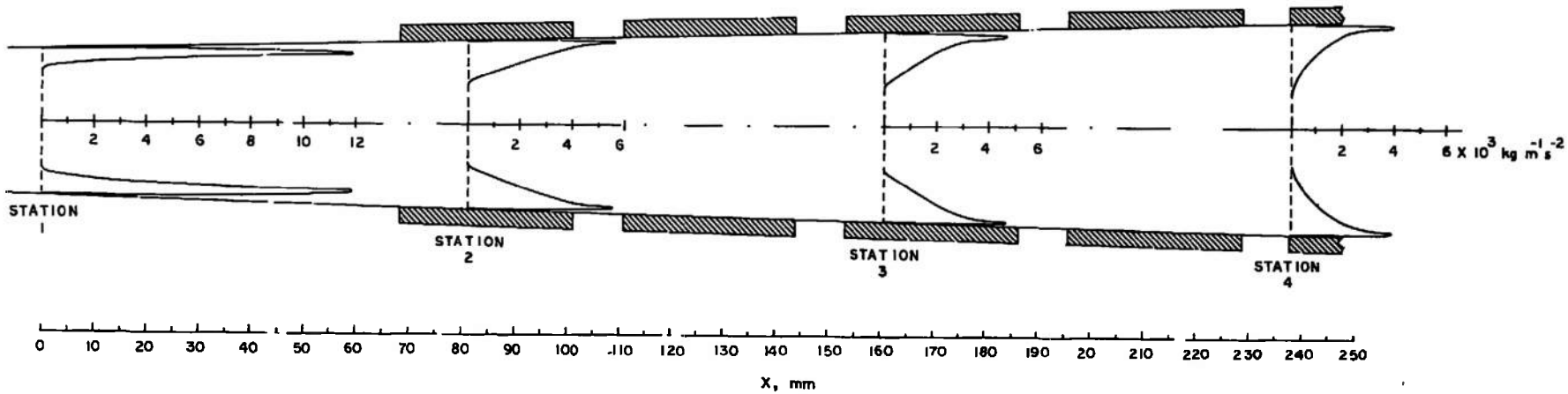

Fig. 6. Development of turbulent shear stress profile in the Hirho accelerator [operating conditions of Run 1412 (Ref. 11)]

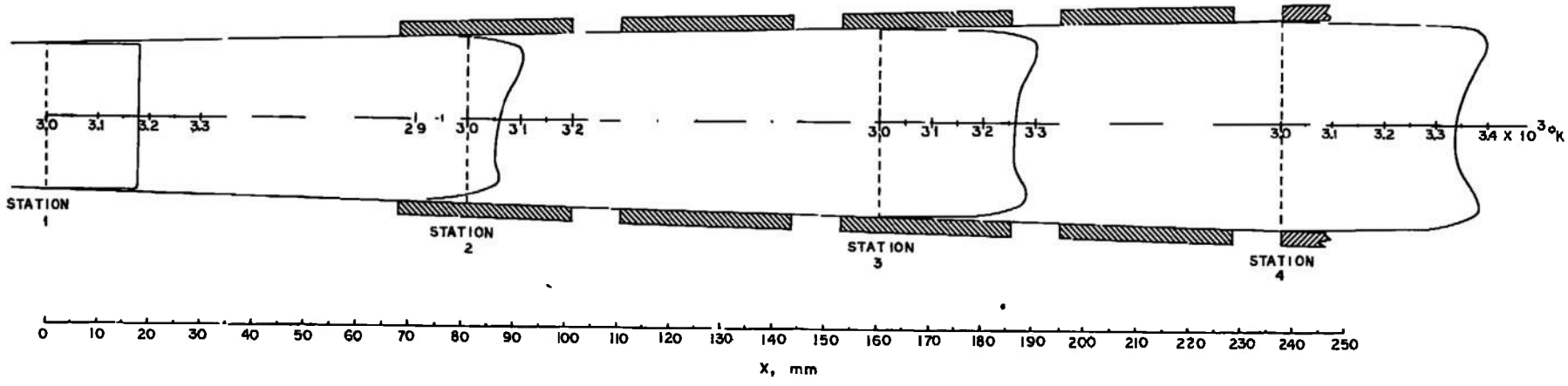

Fig. 7. Development of mean gas temperature profile in the Hirho accelerator [operating conditions of Run 1412 (Ref. 11)]

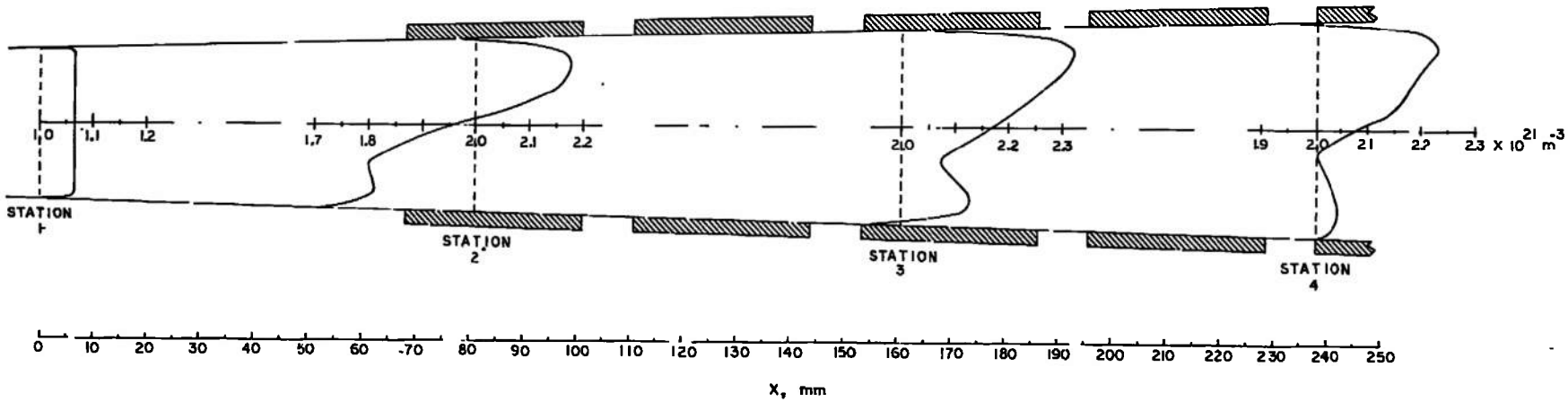

Fig. 8. Development of mean electron number density profile in the Hirho accelerator [operating conditions of Run 1412 (Ref. 11)]

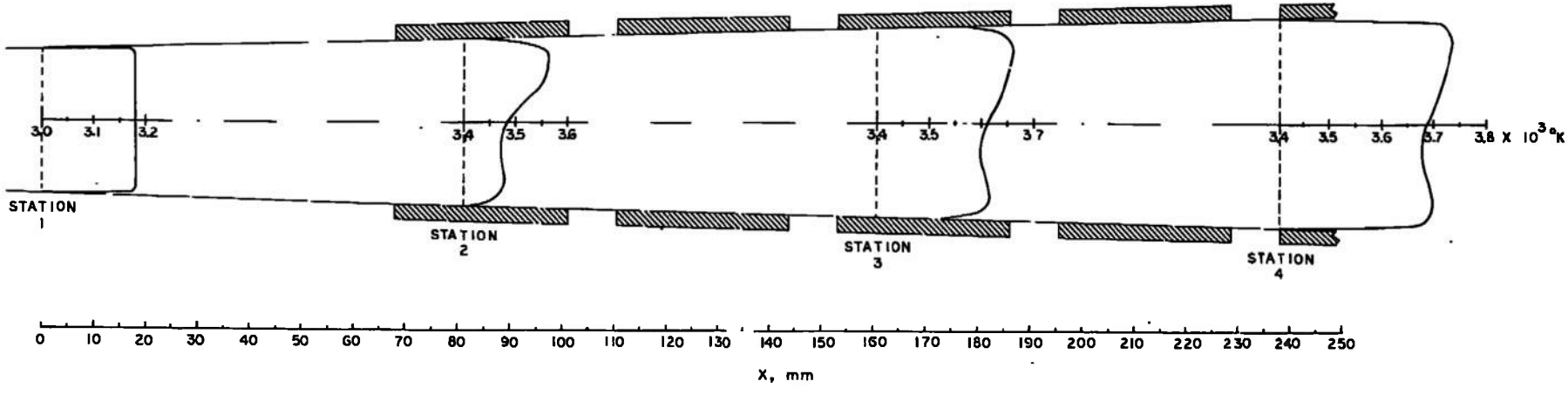

Fig. 9. Development of mean electron temperature profile in the Hirho accelerator [operating conditions of Run 1412 (Ref. 11)]

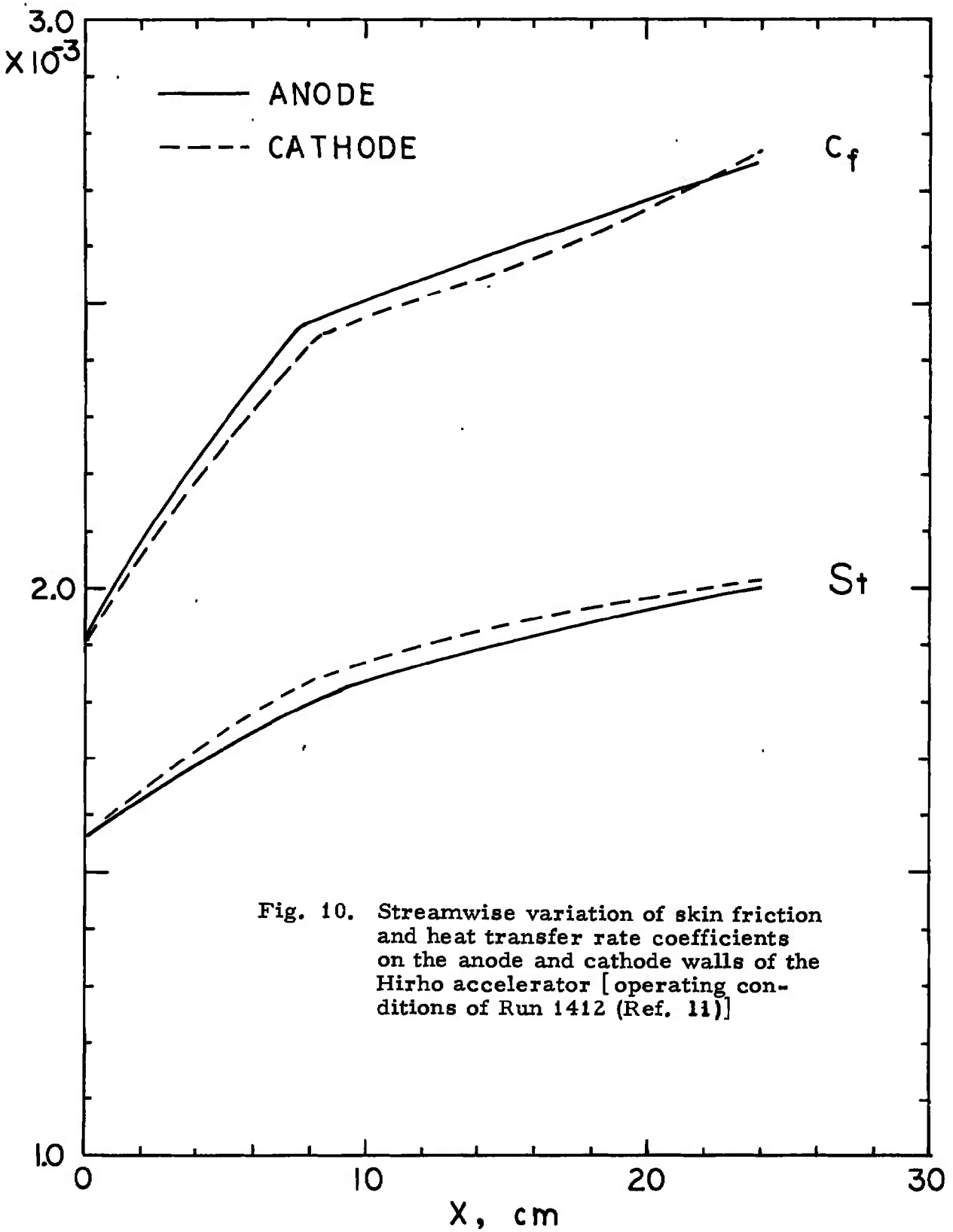

Fig. 10. Streamwise variation of skin friction and heat transfer rate coefficients on the anode and cathode walls of the Hirho accelerator [operating conditions of Run 1412 (Ref. 11)]

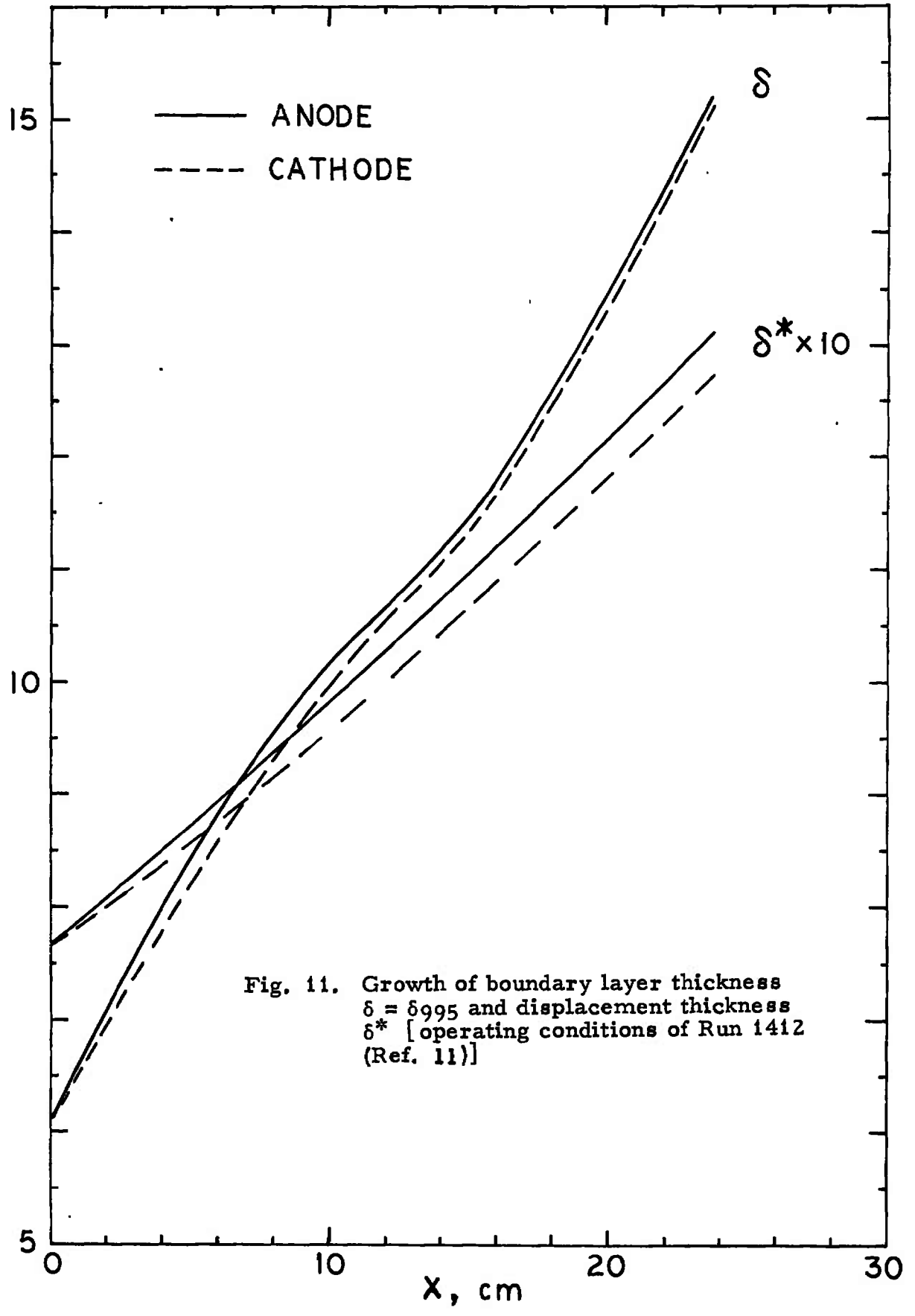

Fig. 11. Growth of boundary layer thickness $\delta = \delta_{995}$ and displacement thickness δ^* [operating conditions of Run 1412 (Ref. 11)]

REFERENCES

1. Argyropoulos, G. S. and Demetriades, S. T., "Current Distribution in Crossed-Field Accelerators (Part II, Effects of Finite Reaction Rates and Electron Energy Convection)," Arnold Engineering Development Center Technical Report AEDC-TR-68-204, September 1968.

2. Argyropoulos, G. S., Casteel, M. A., and Demetriades, S. T., "Current Distribution in Crossed-Field Accelerators (Part III, Electrical and Gasdynamic Performance of J X B Accelerators)," Arnold Engineering Development Center Technical Report AEDC-TR-70-86, March 1970.

3. Demetriades, S. T. and Argyropoulos, G. S., "Ohm's Law in Multicomponent Nonisothermal Plasmas with Temperature and Pressure Gradients," Phys. Fluids 9, 2136-2149 (1966).

4. Demetriades, S. T., Fonda-Bonardi, G., and Argyropoulos, G. S., "Experimental Determination of Collision Cross Sections for Momentum Transfer," AFOSR Final Scientific Report No. 69-2809TR (September, 1969).

5. Demetriades, S. T., "Determination of Energy-Loss Factors for Slow Electrons in Hot Gases," Phys. Rev. 158, 215-217 (1967).

6. Demetriades, S. T. and Maxwell, C. D., "Determination of Energy-Loss Factors for Slow Electrons in Hot Gases," NASA Report No. CR-73400 (1966).

7. Lackner, K., Argyropoulos, G. S. and Demetriades, S. T., "Relaxation Effects in J × B Devices," AIAA J. 6, 949-951 (1968).

8. Argyropoulos, G. S., Demetriades, S. T. and Lackner, K., "Compressible Turbulent Magnetohydrodynamic Boundary Layers," Phys. Fluids 11, 2559-2566 (1968).

9. Demetriades, S. T., "Magnetohydrodynamic Orbit Control for Satellites," Electrical Engineering N. Y., 79, 987 (1960).

10. Argyropoulos, G. S. and Casteel, M. A., "Tables of Interaction Parameters for Computation of Ohm's Law Coefficients in Various Gases," J. Appl. Phys., issue of September 1970.

11. Norman, W., and Siler, L. G., "Experiments on a Shock Tunnel Augmented by a Magnetohydrodynamic Nozzle Accelerator," Arnold Engineering Development Center Technical Report AEDC-TR-68-232, December 1968.

12. Argyropoulos, G.S., Casteel, M.A., and Demetriades, S.T., "Two-dimensional Distribution of Current along Magnetohydrodynamic Channels," Tenth Symposium on Engineering Aspects of Magnetohydrodynamics, Cambridge, Mass., Proceedings, pp. 29-32 (1969).

13. Demetriades, S.T., "Momentum Transfer to Plasmas by Lorentz Forces," Physico-Chemical Diagnostics of Plasmas, T.P. Anderson, R. W. Springer, R. C. Warden, Editors, Northwestern Univ. Press, Evanston, Illinois, 1964, pp. 297-328; also Proceedings of the Fifth Biennial Gas Dynamics Symposium, Northwestern University, Evanston, Illinois, 14-16 August, 1963.

14. Preliminary Proceedings of AFOSR-IFP-Stanford 1968 Conference on Turbulent Boundary Layers (Stanford, 1968), Volume I: Prediction Methods and Physical Structure.

15. Preliminary Proceedings of AFOSR-IFP-Stanford 1968 Conference on Trubulent Boundary Layers (Stanford, 1968), Volume II: Compiled Data.

APPENDIX A
APPLICATIONS OF THE BOUNDARY LAYER SOLUTION TO CASES FOR WHICH EXPERIMENTAL RESULTS ARE AVAILABLE

The novel formulation and method of solution used in this study for the boundary layer problem has been tested carefully for accuracy and reliability by application to well documented cases of turbulent boundary layer flows, for which consistent experimental results were available. For this purpose, test cases were selected among the 33 incompressible turbulent flows documented by D. Coles for the AFOSR-IFP-Stanford 1968 Conference on Turbulent Boundary Layers (Refs. 14 and 15). The experimental results collected for this conference (Ref. 15) and the results of the computations carried out by the participants (Ref. 14) concerned the axial variation of the skin friction coefficient c_f, the shape factor $H = \delta^*/\theta$, and the momentum-thickness-Reynolds number $Re_\theta \equiv U_\infty \theta/\nu$, where δ^* is the displacement thickness, θ the momentum thickness and ν the kinematic viscosity. These particular quantities were selected on the basis that they should provide a more sensitive indication of the accuracy of the prediction method than the overall velocity profile. For the purpose of the conference, values of these quantities were obtained numerically from measured velocity profiles at various axial stations. Specifically, c_f was obtained by fitting the "logarithmic law of the wall" to the experimental velocity profile, and δ^* and θ were calculated using a modified Simpson integration. The predictions reported in Ref. 14 were all started at a specified station in each case, with initial conditions such as to match c_f and Re_θ with the experimental values at that station.

Two of the cases that were selected for testing our method of solution, and which will be described here, were those identified in the conference as cases 2100 and 2400. Case 2100 was subject to an initial mildly negative pressure gradient, which then became strongly positive at about $x = 18$ feet, leading to eventual separation. Case 2400 involved a moderately positive pressure gradient, which dropped abruptly at zero near $x = 5$ feet.

The numerical results obtained for these two cases by the various participants in the conference are shown on Figs. 12 and 16 respectively.

(These figures are reproduced here from Ref. 14.) The results of the new solution method developed in this study are shown on Figs. 13-15 for Case 2100, and on Figs. 17-19 for Case 2400; note that the latter results were obtained by matching the initial values of c_f and of the kinematic viscosity only.

It is clear from Figs. 12-19 that the new method of solution developed in this study gives quite satisfactory results for these two incompressible test cases, and in fact shows up quite well in comparison with any one of the conventional methods. In particular, the results for c_f are in very good agreement with the experimental data.

Results obtained by the new method of solution for the compressible magnetohydrodynamic boundary layer development in the Hirho experiment have been described in the main text.

× Experimental (Ref. 15) —— Theoretical (Ref. 14)

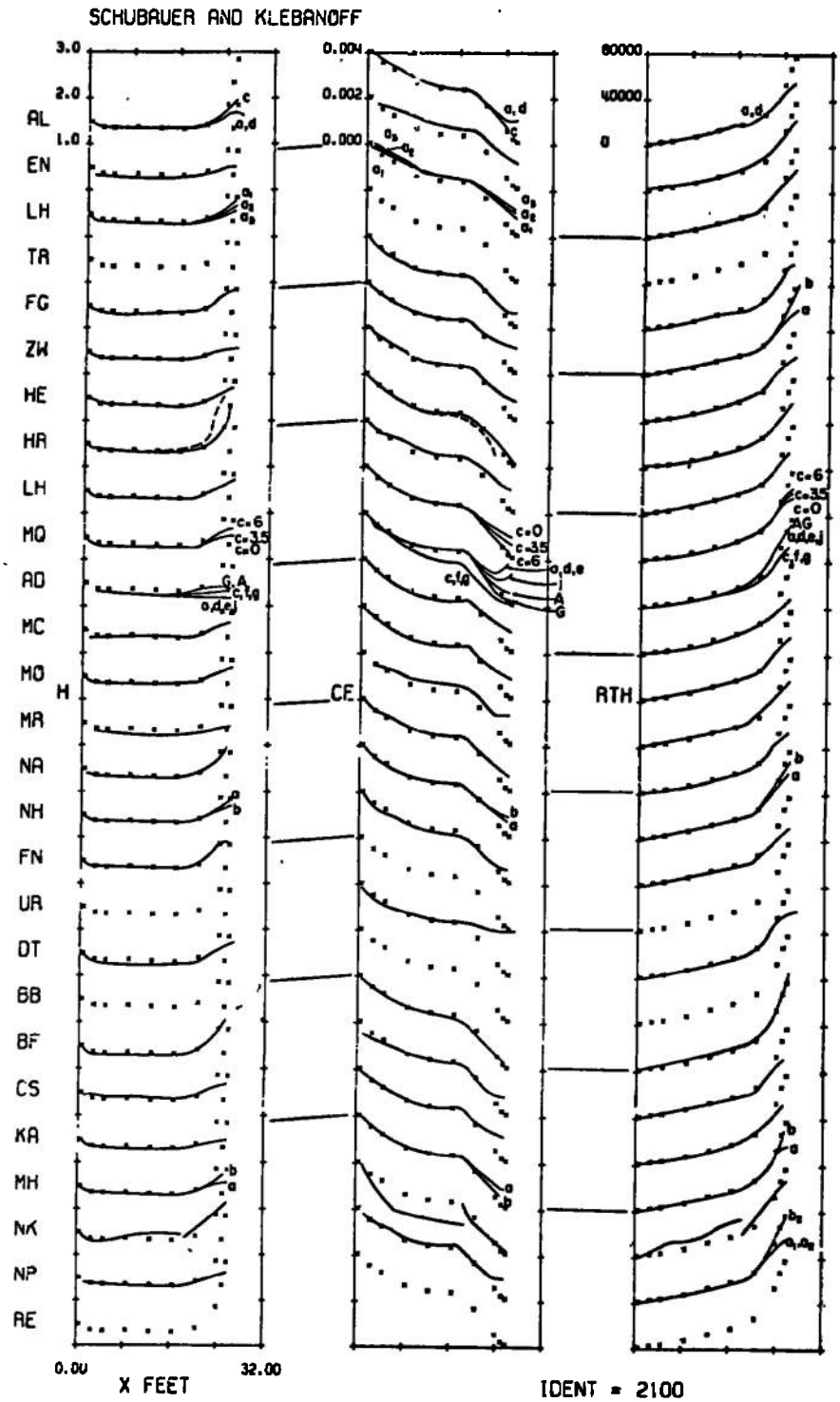

Fig. 12. $H \equiv \delta^*/\theta$, c_f and Re_θ for the conditions of Case 2100

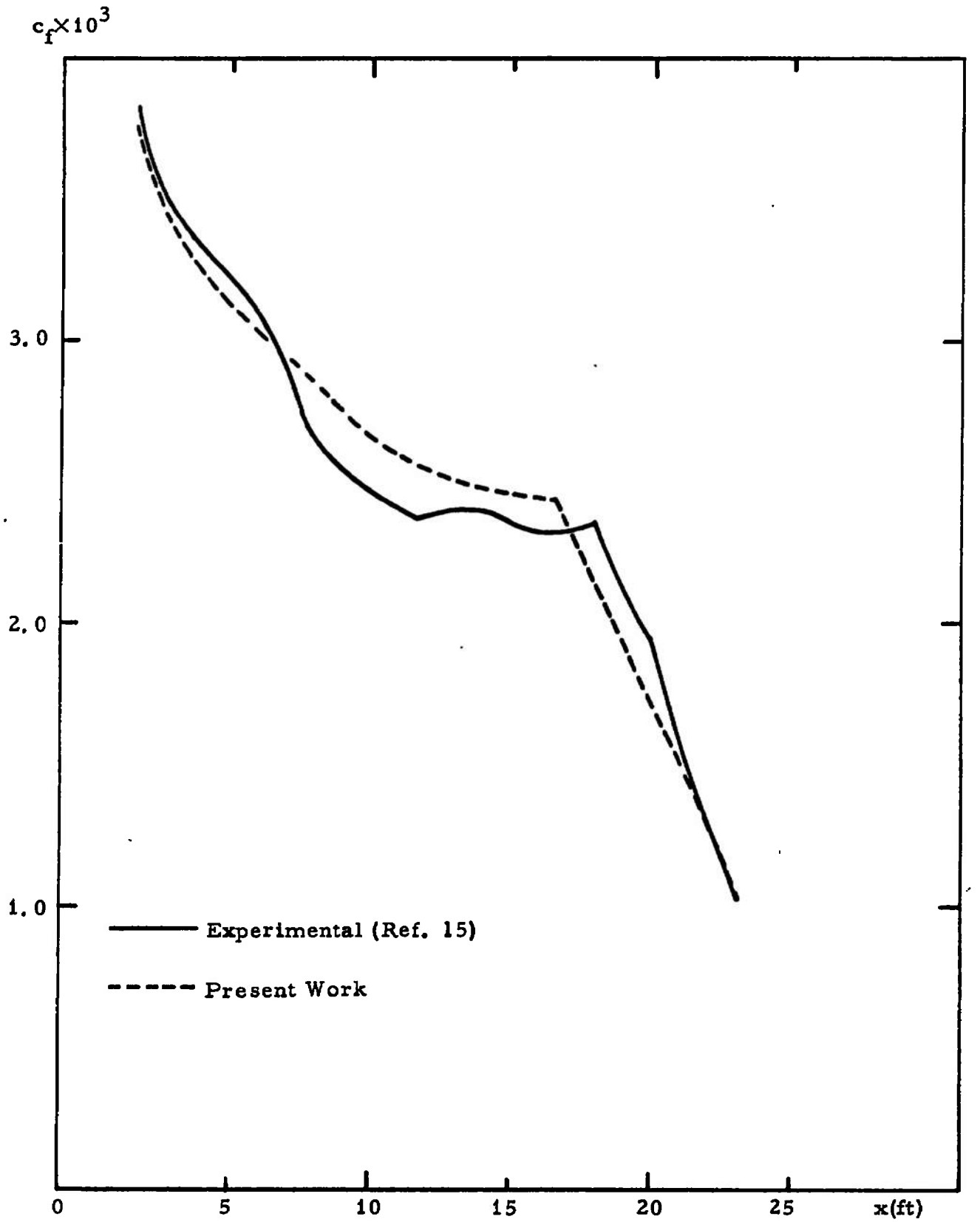

Fig. 13. c_f vs. x for the conditions of Case 2100.

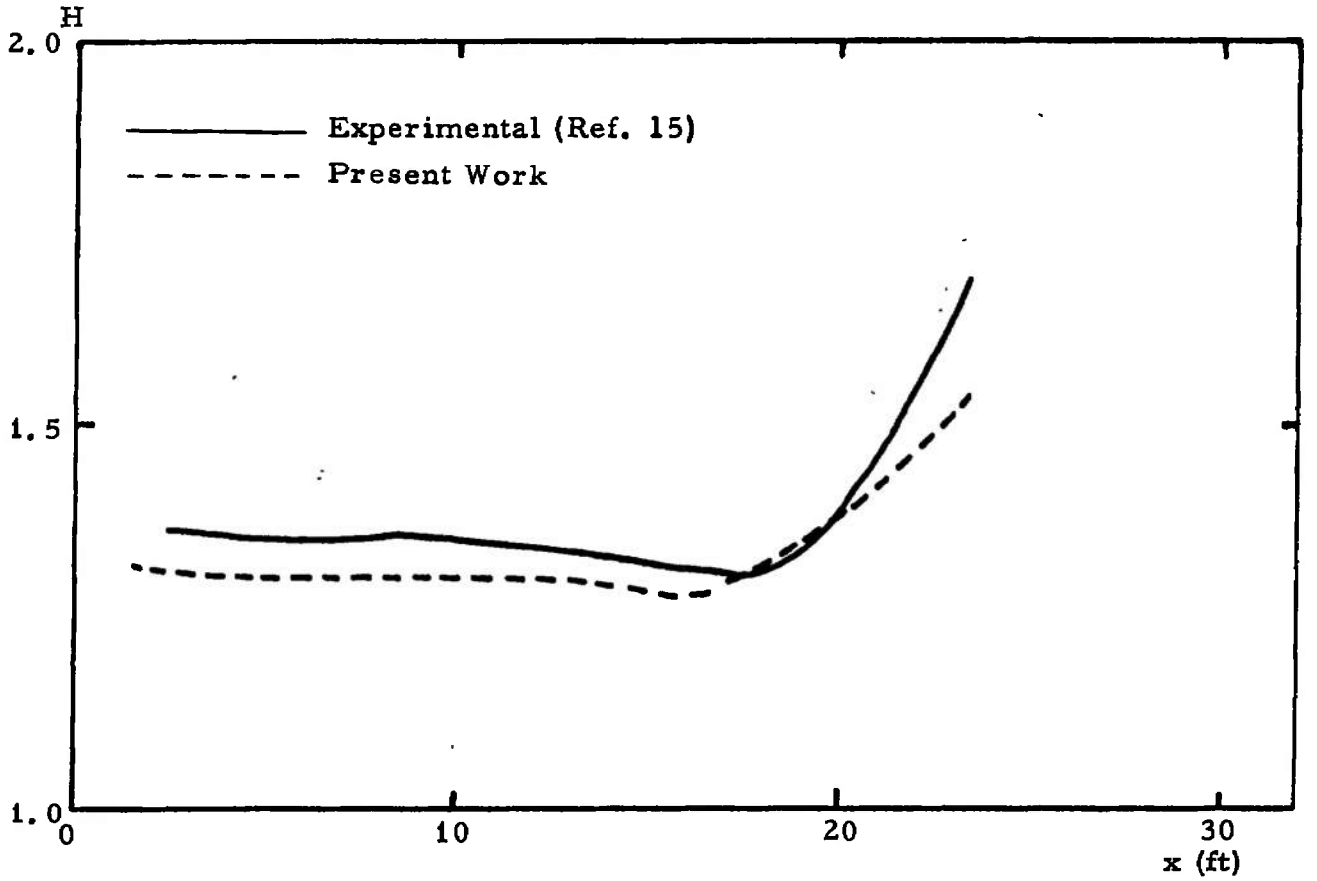

Fig. 14. $H \equiv \delta^*/\theta$ vs. x for the conditions of Case 2100

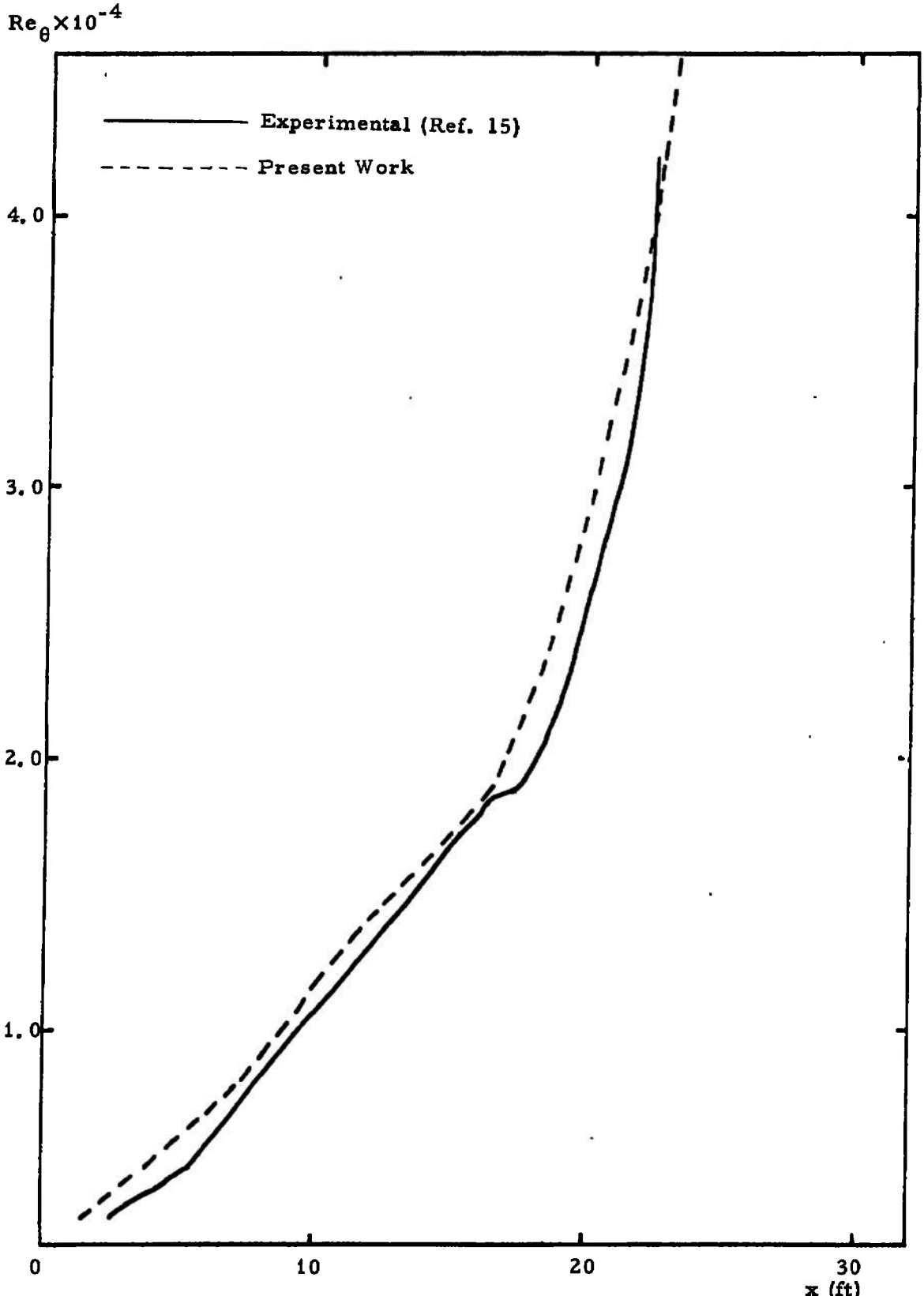

Fig. 15. $Re_\theta \equiv u_\infty \theta/\nu$ vs. x for the conditions of Case 2100

x Experimental (Ref. 15) —— Theoretical (Ref. 14)

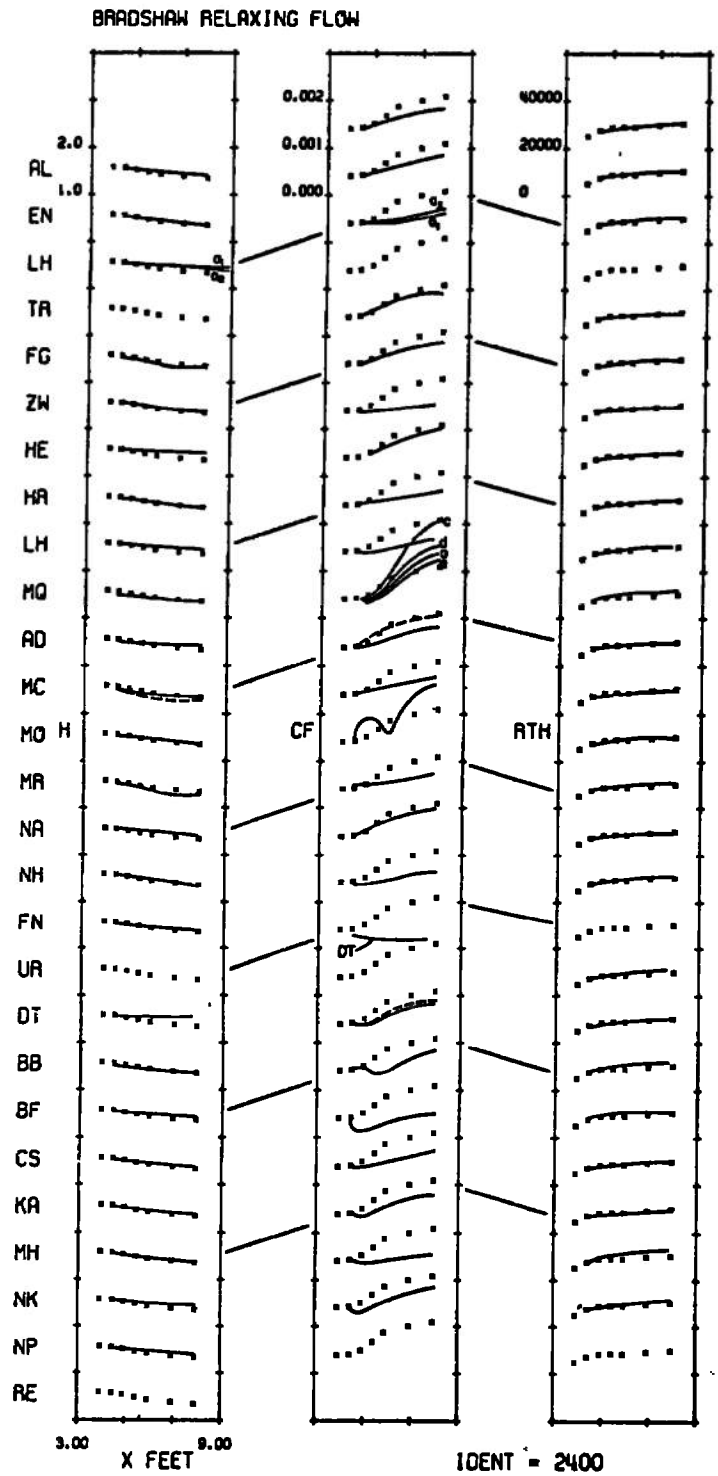

Fig. 16. $H \equiv \delta^*/\theta$, c_f and R_θ for the conditions of Case 2400.

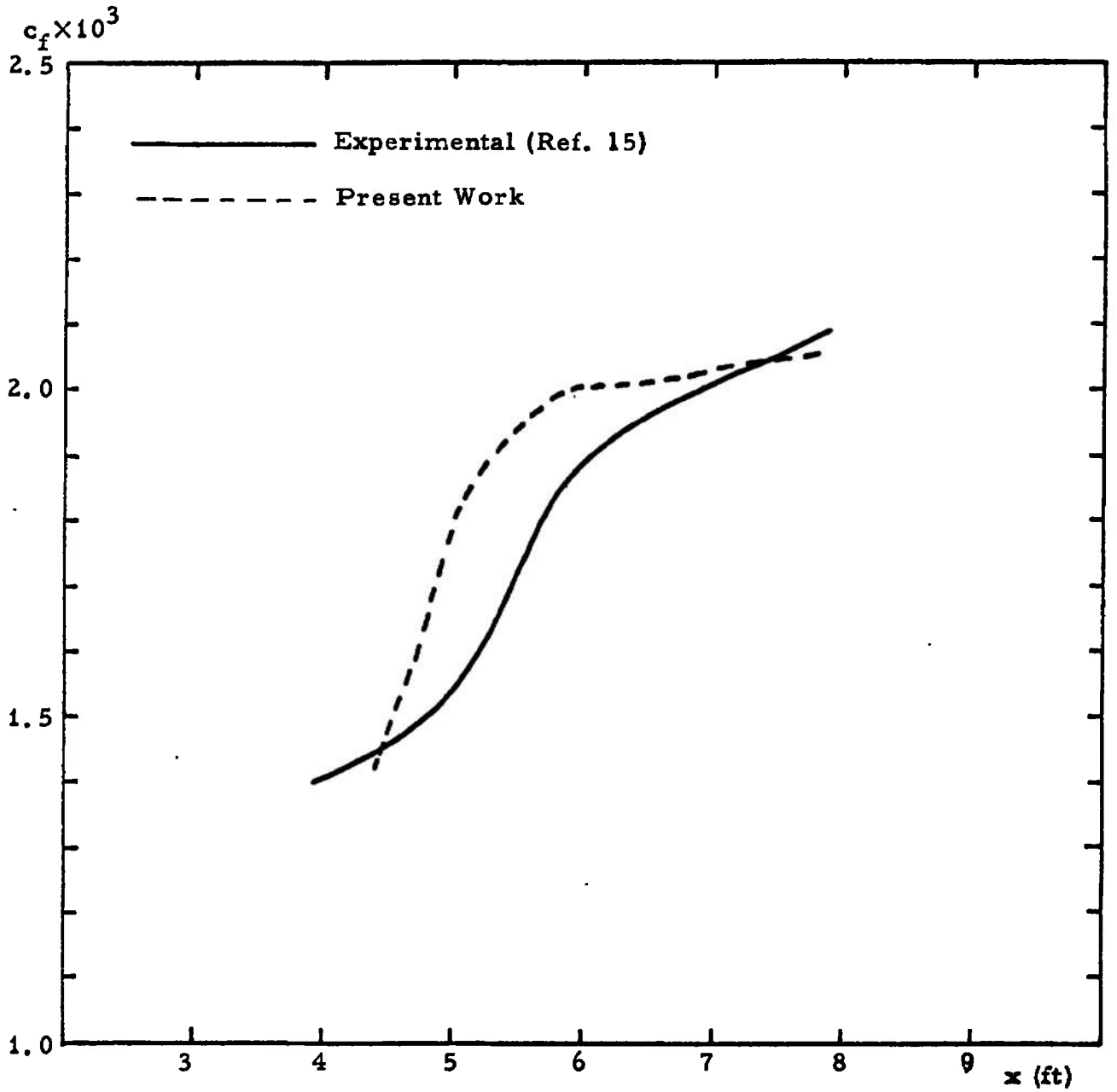

Fig. 17. c_f vs. x for the conditions of Case 2400.

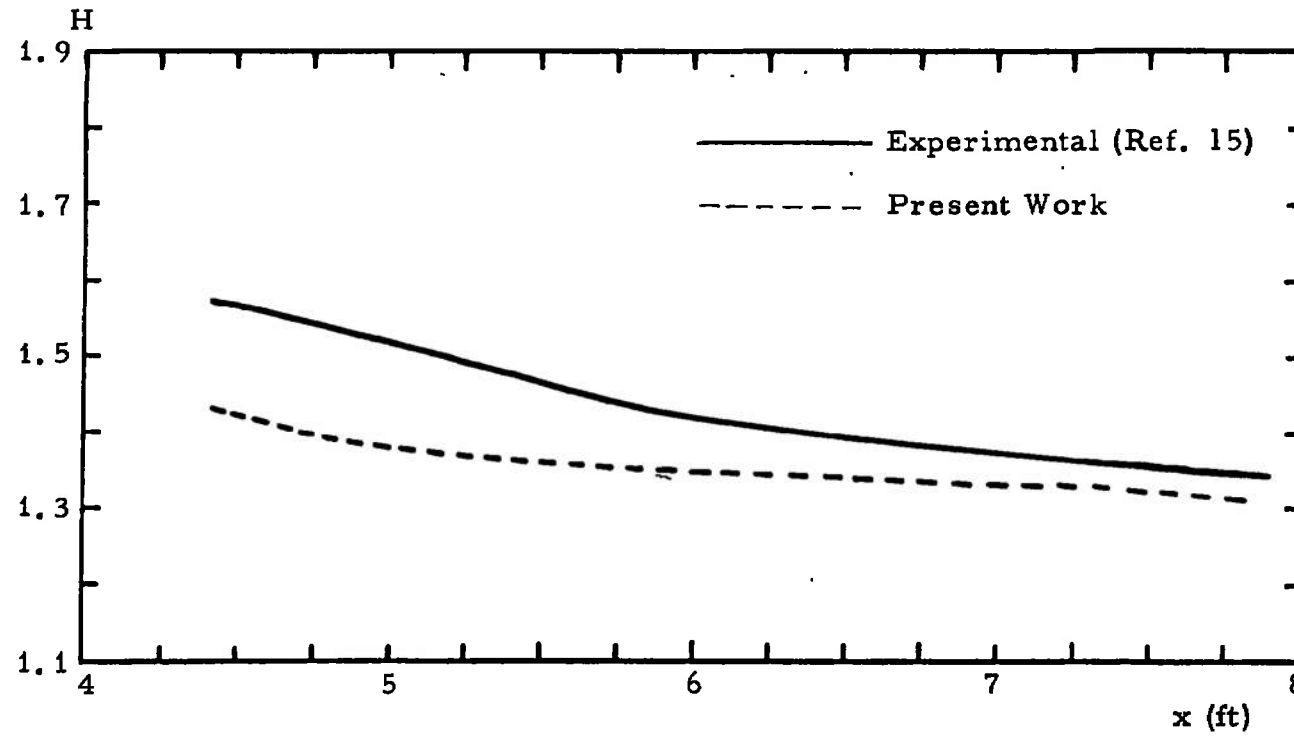

Fig. 18. $H \equiv \delta^*/\theta$ vs. x for the conditions of Case 2400.

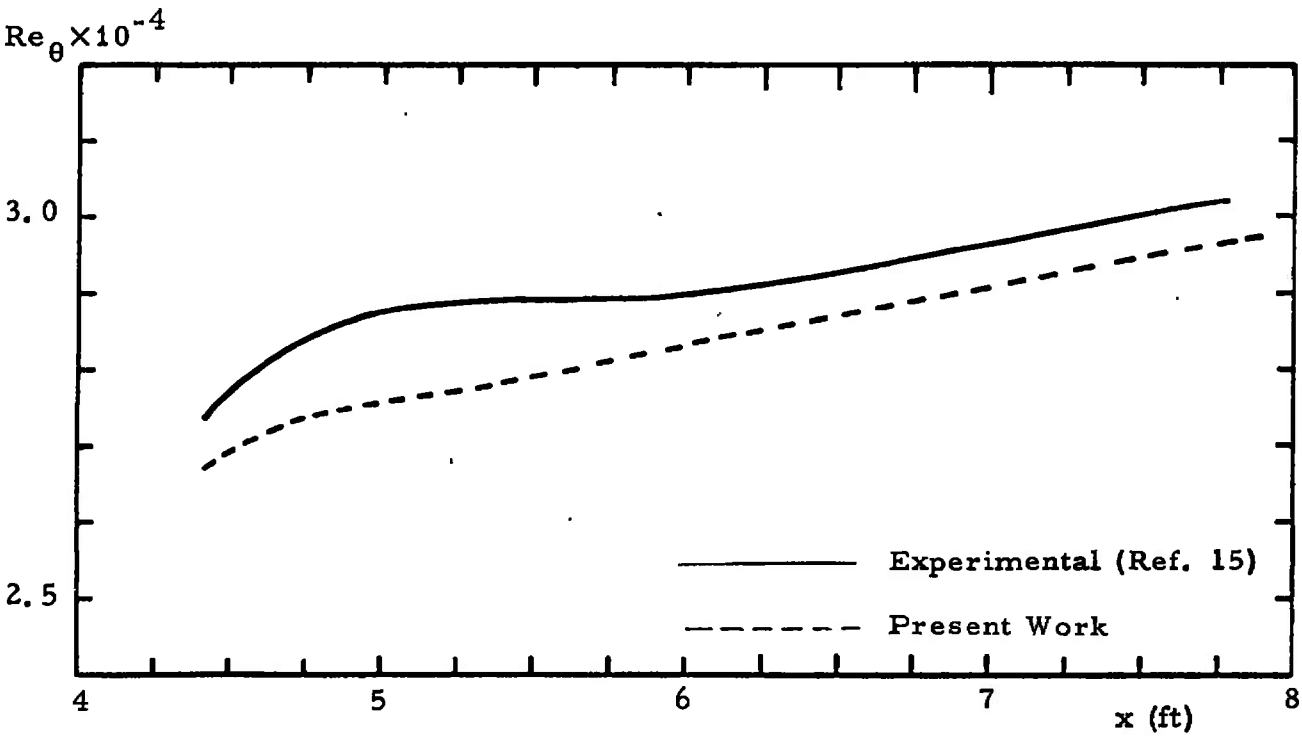

Fig. 19. $Re_\theta \equiv u_\infty \theta/\nu$ vs. x for the conditions of Case 2400.

APPENDIX B

DESCRIPTION OF COMPUTER PROGRAM "COUPLED"

B. 1. GENERAL DESCRIPTION

Program COUPLED has been written to couple the separate solutions of the electrical and gasdynamic problem over any prescribed accelerator length. In other words, this program carries out the iteration described in the main text between the electrical solution (which is carried out by subprogram "INLET" — see Ref. 2) and the gasdynamic solution, which includes quasi-one-dimensional solution in the core of the flow and full two-dimensional computation of the compressible turbulent boundary layers on both the anode and the cathode walls. The boundary layer development on the two electrode walls is carried out by subprogram "BLS," which is essentially a minor modification of the program "LAYER" described in Ref. 2. The user may, at his option, specify solution of the electrical part of the problem alone, or of the coupled problem; in the latter case, the quasi-one-dimensional solution of the gasdynamic problem in the core of the flow is incorporated to the solution of the electrical problem by considering the flow in streamtubes, without viscosity or heat conduction effects.

The solution may be performed over any specified geometry, incorporating up to 20 electrode pairs (powered or unpowered), bounded by insulating walls or insulator segments at the upstream and downstream ends.

The program can treat any working fluid, consisting of as many as 25 separate components formed from up to 10 distinct chemical elements and taking part in up to 50 reactions.

Channel geometry (including dimensions of all conductor and insulator segments, and of leading and trailing insulator walls), axial distribution of magnetic field strength, electric current passed through each electrode pair, and initial profiles of gasdynamic unknowns must all be provided.

The program will then proceed for a specified number of iterations between gasdynamic and electrical solutions, whereupon a restart deck can be generated so that the computation may be continued from this point at a later time.

COUPLED and its subprograms (see Ref. 2) have all been coded in FORTRAN for the Control Data Corporation 6600 computer, requires approximately 100,000 memory locations in core, and utilizes the ability of this computer system to retain 28 significant digits (double precision). Typical computations of a whole duct require approximately 50 seconds of central processor time on the CDC 6600 for each complete (electrical + gasdynamic) iteration cycle. As mentioned in the main text, three or four such cycles are typically needed for convergence.

The following sections provide a user's description of program COUPLED. Section B. 2 describes input data and formats, B. 3 lists optionally available output, B. 4 lists the routines included in the program, and Section B. 5 defines important variable names used in these routines. A listing of the FORTRAN code and a source deck are provided separately.

A. 2. INPUT DATA AND FORMATS

(1) For the electrical part of the solution

Columns	Format	
1-80	10A8	The first card contains the HEADING to be printed at the top of each new page. Leaving columns 1-8 blank terminates the program.
1-24	12I3	The second card specifies the options to be used in the METHODS OF SOLUTION. Each field on this card controls one of the options listed below, and a non-zero punch in this field selects the corresponding option.

OPTION	FIELD #
Logarithmic solution for seed ion	1
Solve for gasdynamic variables u, T along streamlines	2
Compute electric field and potential	3

OPTION	FIELD #
Coupled solution	4
Logarithmic solution for T_e	5
Use implicit algebraic equation for T_e	6
Include effects of thermal and concentration diffusion	7
Impose periodicity over one electrode period as boundary condition on Ψ: If field contains 1, at upstream end If 2, at downstream end	8
Consider seed reaction only	9
Assume instantaneous Saha equilibrium	10
Assume instantaneous electron energy relaxation	11
Assume (10) and (11) during first cycle	12

Columns	Format	
1-3	I3	Number of current density iteration cycles to be performed (up to 25) for the electrical problem (Ref. 1).
1-30	10I3	The fourth card is the INPUT CONTROL card. The remaining input for the electrical problem is separated into nine categories, corresponding to the first nine fields on this card. To select input of these categories a non-zero punch is placed in the appropriate fields. A non-zero punch in the tenth field indicates that a computation in process has been interrupted for input and is now to be continued.

CATEGORY	FIELD #
1. Output control deck	9
2. Specification of working fluid	1
3. Specification of reactions	2
4. Specification of geometry and grid	3

CATEGORY	FIELD #
5. Specification of operating conditions	4
6. Specification of initial profiles for gas velocity, gas temperature, and number density of each gas component	4
7. Specification of axial distribution of gas velocity and temperature	5
8. Specification of electron temperature distribution	6
9. Restart decks of two kinds	7, 8

Category 1 OUTPUT CONTROL

8 of the 26 cards in this category control the options for printing out the current values of variables of interest at the end of each iteration cycle. Each card corresponds to one of the output categories mentioned below, and to select output of any category at the ends of any given cycles, punch the numbers of those cycles (1 through 25) in successive fields on the appropriate card. A non-zero, negative number punched in the first field on any card will select that output at the end of every cycle.

OUTPUT CATEGORY	CARD #
Stream function field	4
Current density field	5
Electron number density field	11
Plasma property fields $\frac{\epsilon}{\sigma}$, $\frac{\beta}{\sigma}$	12
T_e field	13
T_e increment (from previous cycle) field	14
T, u fields	15
Electric field and potential	21

Another 13 cards correspond to debugging output that need not concern us here, and have not been listed.

Columns	Format	
1-75	25I3	Format of each OUTPUT CONTROL card

The next 4 cards in this category control punched output (described in Section A. 3), suitable for computer-generated contour plots of electron temperature or number density, current streamfunction, or electric potential, or for continuing the computation at a later date.

PUNCH CATEGORY	CARD #
Restart decks of two kinds	22, 23
Plot decks of two kinds	24, 25

1-75	25I3	Format of PUNCH CONTROL cards

The last card in this category indicates quantities to be plotted.

1-12	4I3	Quantities for which plot decks are desired are selected by a non-zero punch in the appropriate field on this card

QUANTITY	FIELD #
Electron temperature	1
Electron number density	2
Current streamfunction	3
Electric potential	4

Category 2 WORKING FLUID

1-10	E10. 3	Ratio of specific heats (c_p/c_v)
1-5	I5	Number of elements (up to 10)
6-10	I5	Number of components (up to 25)

Each element is described on a card of the following format

1-10	A10	Name of element
11-20	E10. 3	Atomic weight of element (amu)

Each component is then described on a card of the following format

1-4	A4	Name of component
11-60	10I5	The composition of this component in terms of punching, in the appropriate fields, the number of particles of the corresponding elements contained in each particle of this component

Columns	Format		
1-10	E10.3	Ionization energy of seed ion above its neutral ground state	(eV)

For each neutral component κ, the following transport properties are specified: (1) integrated electron-neutral collision cross section for momentum transfer $Q_{e\kappa}$ and the associated (Ref. 3) weighting factors $A^{(2)}_{e\kappa}$ and $A^{(5)}_{e\kappa}$, (2) ion-neutral cross section $Q_{i\kappa}$ for the prevalent ion i in the gas (i.e., the seed ion in the case of a seeded gas), and (3) the electron-neutral energy loss factors $\delta_{e\kappa}$ (Ref. 5). Categories (1) and (3) are specified in tabular form as functions of electron temperature. Consequently, the range of electron temperature for these tables is specified first, as follows:

1-10	E10.3	Minimum value of T_e for tables	(^oK)
11-20	E10.3	Tabular interval in T_e for tables	(^oK)
21-30	E10.3	Maximum value of T_e for tables	(^oK)

The first table is input in the following format, where one card corresponds to each electron temperature entry:

1-18	18x	May be used for identification	
19-28	E10.3	Electron-neutral cross section	(m^2)
29-38	E10.3	Weighting factor $A^{(2)}$	
39-48	E10.3	Weighting factor $A^{(5)}$	

There follows <u>one</u> card specifying the collision cross section for momentum transfer between the neutral component in question and the prevalent ion, in the format

1-10	E10.3	Ion-neutral cross section	(m^2)

Finally there follows the table of electron-neutral energy loss factor in the following format, where again one card corresponds to each electron temperature entry:

1-10	E10.3	Electron-neutral energy-loss factor

<u>Category 3</u> CHEMICAL REACTIONS

Provision has been made for the specification of up to 50 reactions between the plasma components. Each reaction, which may be written symbolically as

$$\sum_{j=1}^{4} \nu_j a_j \underset{k_r}{\overset{k_f}{\rightleftharpoons}} \sum_{j=1}^{4} \nu'_j a'_j$$

is defined by specifying the components a_j, a'_j taking part, their stoichiometric coefficients ν_j and ν'_j, the reverse reaction rate constant k_r, and the equilibrium constant $K \equiv k_f/k_r$. The rate constant k_r is specified as a function of temperature either in tabular form or by the expression $k_r = AT^B \exp(C/T)$, and the equilibrium constant K by the expression $K = A'T^{B'}R(T) \exp(C'/T)$. $R(T)$ is the ratio of partition functions of the components on the right-hand side to those on the left-hand side, and is given in tabular form. The forward reaction constant may then be written: $k_f = AA'T^{(B+B')}R(T) \exp[(C+C')/T]$. Specification of the reverse reaction rate constant k_r is done for each reaction as follows:

Columns	Format	
1-10	E10.3	Coefficient A
11-20	E10.3	Coefficient B
21-30	E10.3	Coefficient C

If coefficient A is specified as <u>negative</u>, this is a signal that the analytical expression $k_r = -AT^B \exp(C/T)$ is used for this reaction. If coefficient A is specified as <u>positive</u>, this is a signal that a <u>table</u> will be used for k_r; then the coefficients A, B, and C, that have been specified on this card, have the meaning of the maximum, minimum, and increment, respectively of the independent variable T_e of the table, and the program proceeds to calculate the number of entries corresponding to such a table and then to read as many cards in the format

1-10	E10.3	Rate coefficient k_r

If the coefficient A is <u>zero</u>, this is the signal that all pertinent reactions have been specified and that the inputing of Category 3 has been completed.

The ratio of the partition functions R(T) is specified for only one reaction: the three-body ionization-recombination reaction of the seed. It is input in the way specified above by considering it as an additional k_r. In other words, the quantities specified in Category 3 are one more than the number of reactions, the last one being the ratio R(T) for the seed reaction.

Category 4 GEOMETRY AND GRID

Columns	Format		
1-3	I3	Number of rows	(max. 31)
4-6	I3	Number of columns	(max. 81)
7-9	I3	Number of electrodes	(max. 20)

x- and y-spacings of the grid may be functions of x and y, respectively. In that case, the number of cards read will equal either the number of x-spacings or the number of y-spacings, whichever is greater. A uniform grid may be specified by providing a single card with the negative of the desired x-spacing in the first field and the desired y-spacing in the second.

1-10	E10.3	Desired x-spacing	(m)
11-20	E10.3	Desired y-spacing	(m)
1-80	26I3, I2	Electrode geometry for the wall y = 0, specified by giving the number of grid spaces covered by the leading insulator, first conductor segment, next insulator segment, etc. More than one card may be required.	
1-80	26I3, I2	Electrode geometry for the wall y = D, as above.	
1-30	3E10.3	Quadratic polynomial coefficients W_o, W_1, W_2 for z-dimension of channel $W = W_o + W_1 x + W_2 x^2$ (Needed for the quasi-one-dimensional solution of the problem in the core of the flow.)	(m)

Category 5 PROBLEM PARAMETERS

1-10	D10.3	Total current in x-direction	(A/m)
11-20	D10.3	Streamfunction value on downstream insulator	(A/m)
1-80	8E10.3	Array of values of B, one value per grid column	(Wb/m^2)
1-80	8D10.3	Total current flowing through each electrode pair	(A/m)

Columns	Format		
1-80	8D10.3	Given values of streamfunction on each grid row at column 1 (if required)	(A/m)
1-80	8D10.3	Given values of streamfunction on last column (if required)	(A/m)
1-10	E10.3	Allowable relative variation in T_e	
11-20	E10.3	Allowable relative variation in n_e	
21-30	E10.3	Allowable relative variation in U	
31-40	E10.3	Allowable relative variation in T	
1-10	E10.3	Initial gas pressure	(atm)
11-20	E10.3	Value of T for initial current density calculation	(^oK)
21-30	E10.3	Value of T_e for initial current density calculation	(^oK)
31-40	E10.3	Seed fraction by weight	
41-50	E10.3	Geometrical factor for estimating an initial uniform T_e	
1-10	E10.3	Allowable relative error in T_e for algebraic solution	
11-13	I3	Maximum number of iterations allowed in algebraic solution for T_e	
	Category 6	INITIAL PROFILES	
1-80	8E10.3	Initial values of electron temperature and of all component number densities on rows (by row) For uniform profile, make the first field (i.e., T_e) of row 1 specifications negative.	(^oK) (m^{-3})
1-80	8E10.3	Initial profile of T For uniform profile place negative value ($-T_o$) in the first field.	(^oK)
1-80	8E10.3	Initial profile of U For uniform profile place negative value ($-U_o$) in the first field.	

Category 7 AXIAL VARIATION OF U, T ON CENTERLINE

Columns	Format		
1-80	8E10.3	Values of T_{CL} for all columns For uniform distribution place ($-T_{CL}$) in the first field.	(^{o}K)
1-80	8E10.3	Values of U_{CL} for all columns For uniform distribution place ($-U_{CL}$) in the first field.	(m/s)

Category 8 ELECTRON TEMPERATURE DISTRIBUTION

1-80	8E10.3	Values of electron temperature for all grid points First row-first column, first row-second column, etc.	(^{o}K)

Category 9 RESTART DECK

As suitable for each field		Read restart deck as punched by INLET

(2) For the coupled boundary layer

1-3	I3	Number of iteration cycles to be used for the solution of the coupled problem. If zero, the boundary layer development is not computed, and execution stops after completion of the electrical solution.
4-6	I3	Flag for punching restart deck. If this flag is zero, no restart deck is punched at the end of the solution of the coupled problem that is to be performed by this run.
1-40	4A10	Contains the heading to be printed at the top of every page of printout pertaining to the boundary layer solution.

Columns	Format		
1-10	E10.3	Starting value of the axial variable x	(m)
11-20	E10.7	Interval for x-stations at which the boundary layer profiles of all quantities will be printed out	
1-3	I3	Desired number of sub-intervals across each boundary layer to be used in the boundary layer solution	
4-6	I3	Number of differential equations solved simultaneously by the boundary layer solution	
7-9	I3	Number of iterations performed at each step of the boundary layer solution for the purpose of more accurate estimate of the source terms	
1-10	E10.3	Initial value of free-stream velocity	(m/s)
11-20	E10.3	Initial value of free-stream temperature	(^{o}K)
21-30	E10.3	Initial value of static pressure	(atm)
31-40	E10.3	Wall temperature	
41-50	E10.3	Initial boundary layer thickness	(m)
51-60	E10.3	Seed fraction (by weight)	
61-70	E10.3	Total mass flow rate in channel	(kg/s)
71-80	E10.3	Effective energy loss factor for electron-neutral collisions in the specified mixture	
1-10	E10.3	Constant factor A in the expression $k_r = AT^B \exp(C/T)$ for the three-body recombination reaction of the seed	
11-20	E10.3	Exponent B in the above expression	
21-30	E10.3	Allowable relative error in T_e in the algebraic solution of the electron energy equation	

Columns	Format	
1-10	E10.3	Approximate boundary layer thickness estimated at the final x-station of the geometry, to be used only for the purpose of initiating the coupled solution

The next card specifies the allowable relative variation in the x-direction of the free-stream values of each unknown; they are used to control the x-step during the boundary layer solution.

1-50	5E10.3	Allowable relative free-stream variation of u, T, n_e, T_e, and τ respectively
1-10	E10.3	Exponent α in expression for initial profile of y: $y_i = \delta(i/N)^{\alpha}$ $i = 0...N$
11-20	E10.3	Exponent β in expression for initial profile of gas velocity: $U_i = U_\infty(y_i/\delta)^{\beta}$ $i = 0...N$
21-30	E10.3	Exponent γ in expression for initial profile of gas temperature: $T_i = T_w + (T_\infty - T_w)\cdot(y_i/\delta)^{\gamma}$ $i = 0...N$

If the exponent α for the profile of y is zero, the following group of cards is input

1-80	8E10.3	Table of values of y_i/δ $i = 0...N$

If the exponent β for the velocity profile is zero, the following group of cards is input

1-80	8E10.3	Table of values of U_i/U_∞ $i = 0...N$

If the exponent γ for the temperature profile is zero, the following group of cards is input

1-80	8E10.3	Table of values of T_i/T_∞ $i = 0...N$

Finally, in case the computation at hand is a continuation (for the same geometry and conditions) of a previously performed run (i.e., if we are "restarting"), then (and only then) the axial variation of the boundary layer thickness on both the anode and cathode walls are specified. This is accomplished by giving the row of the grid (specifically of the grid defined in INLET) nearest to which the free-stream lies:

Columns	Format	
1-75	25I3	Number of grid row near which the free stream of the anode boundary layer is to be found. (More than one card may be required.)
1-75	25I3	Number of grid row near which the free stream of the cathode boundary layer is to be found. (Same number of cards as above will be required.)

B.3. AVAILABLE OUTPUT

(1) From the electrical part of the solution

Both printed and punched output are available from INLET, the latter to provide for continuing a calculation after interruption or to facilitate computer plotting of important quantities.

Printed output, besides giving the values at all points of any quantities requested in Category 1 of input, always collects and prints values of:

Root-mean-square variation of electron temperature between present and previous iteration cycle

Minimum electron temperature

Maximum electron temperature

Number of points where T_e is approaching a steady value from cycle to cycle ("converging")

J_y at trailing edge of the middle electrode at $y = 0$

J_y at leading edge of the middle electrode at $y = D$

Maximum J_y on centerline, and the angle between the current vector and the y-axis at this point

Minimum J_y on centerline, and the angle between the current vector and the y-axis at this point

Hall potential between first and last columns

Punched output varies in form according to the equipment to be used for plots or the method to be used for restarting. For the currently used CALCOMP equipment, each plot deck contains one card for each grid point:

Columns	Format		
4-13	F10.5	x-coordinate of this grid point (relative to first column)	(m)
14-23	F10.5	y-coordinate of this grid point (relative to first row)	(m)
24-33	F10.1	Value of chosen quantity at this grid point	

The restart deck contains values of all the unknown quantities required to continue a calculation. It should be placed as a unit at the end of the input deck for INLET. Care should be taken that the input deck specifies the same working fluid, geometry and grid as the original computation.

(2) From the coupled boundary layer solutions

The values of the normalized cross-coordinate ω, as calculated from the initial profiles, are printed on the first page of output each time that either the anode or the cathode boundary layer are solved for. Then, at each x-station for which output is requested, the program prints out both values of quantities that are independent of the cross-coordinate y and the profiles of important quantities dependent on y.

Quantities independent of cross-coordinate y

Value of x-coordinate
State pressure, p
Current density components, J_x and J_y
Displacement thickness, δ^*
Shape factor, δ^*/θ
Mass flow through boundary layer
Magnetic field, B
Wall temperature, T_w
Momentum thickness, θ
x-Reynolds number, Re_x
Pressure gradient, dp/dx
Displacement thickness Reynolds number, Re_{δ^*}
Momentum thickness Reynolds number, Re_θ
Wall heat flux, $J_{H,w}$
Wall shear stress, τ_w
Skin friction coefficient, $c_f \equiv \tau_w / \frac{1}{2} \rho_\infty U_\infty^2$
Heat transfer coefficient, $St \equiv J_{H,w} / \rho_\infty U_\infty (H_\infty - H_w)$

Quantities dependent on cross-coordinate

Distance from wall, y	Gas velocity, u
Gas temperature, T	Electron temperature, T_e
Mass density, ρ	Electron concentration, c_e
Mach number, M	Ionization relaxation length, L_R
Pressure gradient, $\partial p/\partial x$	Total enthalpy, H
Eddy viscosity, ν_T	Electric field components, E_y, E_x
Ohm's Law coefficients, σ, β, ϵ	Electric number density, n_e
Energy relaxation length, L_E	Electron energy, $c_e h_e$
Static enthalpy, h	Turbulent shear stress, τ

B. 4. ROUTINES USED IN PROGRAM COUPLED

The main program COUPLED performs only the control function for carrying out the iteration between the electrical and gasdynamic parts of the problem.

It calls two sub-programs, INLET, and BLS, and three subroutines, SETBLS, PRSD, and PDELTA.

The first subprogram (INLET) performs the input, output and the tasks involved in the electrical part of the problem.

The subroutine SETBLS performs the input for the boundary layer solutions and initializes the profiles and the boundary layer thickness.

The second subprogram (BLS) controls the computation of the turbulent boundary layer development on both the anode and cathode walls.

It is clear that SETBLS will be called once, while INLET and BLS will be called alternatively as many times as the number of iterations that are to be performed between the electrical and gasdynamic part of the problem.

While INLET is treated as a subroutine of COUPLED, the sub-program BLS is made into an OVERLAY (1, 0) which, when called by COUPLED, is loaded at the beginning of the latter's blank common.

After the iteration for the coupled solution is completed, the main program COUPLED has the option of calling the subroutines PRSD and PDELTA to punch a restart deck.

In the following we shall list the subroutines used in the execution of each of the subprograms INLET and BLS. The list will include a short description of the function of each routine, and the following symbols will be used: P = program, S = subroutine, and F = function subroutine.

(1) Subprogram INLET

ROUTINE		FUNCTION
INLET4	P	Controls input, printing of input data, initializing of variables and performance of the first solution of the electrical part of the problem
INLET	P	Controls subsequent solutions of the electrical part of the problem in the iteration for the coupled solution
OP	S	Performs all printing output
IP	S	Performs all input
SETUP	S	Performs tasks associated with initializing or continuing a problem
PRPGTE	S	Principal routine in solution of finite-difference equations for streamfunction
SPREAD	S	Subordinate to PRPGTE
PSF	S	Calculates values of streamfunction after PRPGTE has achieved solution
CDCF	S	Calculates current density field by differentiation of streamfunction
ANODE	S	Calculates elements of finite-difference coefficient array along wall at $y = 0$
CORE	S	Calculates elements of finite-difference coefficient array away from walls
CATHODE	S	Calculates elements of finite-difference coefficient array along wall at $y = D$
HALL	S	Calculates plasma properties for a given set of conditions
TAND	S	Performs solution for gasdynamic variables (U, T, T_e, n_a) along streamlines

ROUTINE		FUNCTION
TTEST	S	Compiles and evaluates general characteristics
POTENT	S	Calculates electric field and potential
COMPOS	S	Calculates plasma composition at Saha equilibrium
RK	F	Calculates reaction rate constants
DIFTE	F	Evaluates dT_e/dx for use in TAND
E	F	Iterative solution of implicit algebraic equation for T_e
F	F	Iterative solution of implicit algebraic equation for T_e
ANEWTE	F	Subordinate to E, F
PVAL	F	Table lookup function
MATINV	S	Matrix inverter
PDECK	S	Performs all punched output
PROP	S	Calculates plasma properties all along a grid row
RELAX	S	Evaluates relaxation lengths and stabilities
DZ	F	Evaluates z-dimension of channel

(2) Subprogram BLS

BLS	P	Controls the computation of the turbulent boundary layer development on the anode and cathode walls
INTOBL	S	Transmits information from the available solution of the electrical part of the problem into arrays that will be used for the boundary layer solution
BLTOIN	S	Stores information during the computation of the boundary layer development to be used in the subsequent solution of the electrical part of the problem
BL	S	Controls the computation of the boundary layer development on one wall. Its argument signifies anode when it is equal to 1, and cathode when it is equal to 2
EEE	S	Controls iterative solution of implicit algebraic equation for T_e
E	F	Performs iterative solution for T_e
INV	S	Matrix inverter (2 × 2)

ROUTINE		FUNCTION
F	F	Performs iterative solution for T_e
ANEWTE	F	Subordinate to E and F
BEGIN	S	Performs tasks associated with initiating or continuing computations
COEFF	S	Calculates finite-difference coefficients away from the wall and freestream boundaries
COMPOS	S	Calculates plasma composition at Saha equilibrium
CONSTS	S	Defines constants to be used throughout the boundary layer computation
ENTRN	S	Evaluates mass entrainment term $\dot{m}_E$
LENGTH	S	Calculates boundary layer thickness, δ_{995}, and turbulence correlation functions a_2 and a_3
OHM	S	Calculates electric field components E_x and E_y
OUTPUT	S	Performs all output
PAIR	S	Calculates static enthalpy as a function of pressure and temperature for air
PAPH	S	Calculates temperature as a function of pressure and static enthalpy for air
PRE	S	Calculates the pressure gradient at each x-station
PROP	S	Calculates Ohm's law coefficients σ, β, ϵ and associated quantities
READY	S	Calculates distance from wall for each grid point
SLIP	S	Calculates finite-difference coefficients for points at wall and freestream boundaries
SOLVE	S	Performs solution of finite-difference equations
SOLVETU	S	Performs solution of coupled finite-difference equations for u, τ
SOURCE	S	Evaluates source terms for all equations
VEFF	S	Evaluates "eddy viscosity"
VISCO	F	Calculates molecular viscosity
WALL	S	Controls Couette-flow solutions
WF1	S	Performs Couette-flow solution for velocity
WF3	S	Performs Couette-flow solutions for other unknowns

B. 5. IMPORTANT VARIABLE NAMES

This list defines the important variable names used internally by the FORTRAN code of each of the two subprograms. Dimensions assigned to arrays are given in parenthesis. An asterisk * indicates double precision arrays.

(1) Subprogram INLET

VARIABLE NAME		DEFINITION	
A(1659, 5)	*	Array of finite-difference coefficients	
ARRAY (81, 80)	*	Recursion array 1	
AIXA	*	Total current in x-direction	(A/m)
AIA(20)	*	Total current through each electrode	(A/m)
AJX(31, 81)		J_x field	(A/m^2)
AJY(31, 81)		J_y field	(A/m^2)
ALC(20)		Lengths of conductor segments on wall at y = 0	(m)
ALCC(20)		Lengths of conductor segments on wall at y = D	(m)
ALI(20)		Lengths of insulator segments on wall at y = 0	(m)
ALIC(20)		Lengths of insulator segments on wall at y = D	(m)
ALO		Length of leading insulator on wall at y = 0	(m)
ALOC		Length of leading insulator on wall at y = D	(m)
AN(25)		Current values of number densities at a point	(m^{-3})
ANEF(31, 81)		Electron number density field	(m^{-3})
ANIC(25, 31)		Initial values of number densities	(m^{-3})
BARRAY(81, 80)	*	Recursion array 2	
BF		Magnetic induction	(Wb/m^2)
BETOSIG(31, 81)		Ohm's law coefficient ratio β/σ	
CP		Specific heat c_p	
CRIT		Critical value of β/ϵ	

VARIABLE NAME	DEFINITION	
D	y-dimension of channel	(m)
EL	Electron energy relaxation length	(m)
EPSOSIG(31, 81)	Ohm's Law coefficient ratio ϵ/σ	
EX(31, 81)	E_x field	(v/m)
EY(31, 81)	E_y field	(v/m)
HX(81)	x-spacing of grid	(m)
HY(31)	y-spacing of grid	(m)
ICYCLE	Iteration cycle count	
KELECT	Number of electrodes in region	
M2	Number of grid rows	
N	Number of grid columns	
NCYCLE	Number of iteration cycles to be performed	
S(2449) *	Streamfunction field	(A/m)
TA(31, 81)	Gas temperature field	(^oK)
TE(31, 81)	Electron temperature field	(^oK)
U(31, 81)	Gas velocity field	(m/s)

(2) Subprogram BLS

AMACH(43)	Mach number at each grid point	
BARA(81)	Free-stream values of the magnetic field	(Wb/m^2)
BETAE(43)	Ohm's law coefficient β_e	
BF	Magnetic field strength, local	(Wb/m^2)
CF	Friction coefficient c_f	
CH	Heat transfer coefficient St	
DDIS	Displacement thickness δ^*	(m)
DMOM	Momentum thickness θ	(m)
DX	Current interval in x for calculation	(m)
EPSE(43)	Ohm's law coefficient ϵ_e	
EX(43)	Electric field component E_x	(v/m)
EY(43)	Electric field component E_y	(v/m)

VARIABLE NAME	DEFINITION	
F(43, 5)	Array of unknowns. F(i, j), i = 1 to N + 2, are the profiles of: j = 1 u; j = 2 H (= $h + u^2/2$); j = 3 c_e (= $m_e n_e/\rho$); j = 4 c_e/h_e (= $5kn_eT_e/2\rho$); j = 5 τ/ρ	
FLUX(3)	Wall flux of H, h_e, c_e	
HSTAT(43)	Static enthalpy, h	(J/kg)
N	Number of intervals across boundary layer	
OM(43)	Values of normalized coordinate ω	
PEI	Mass flow through boundary layer	(kg/(ms))
PJXARA(81)	Free-stream values of current density component J_x	(A/m^2)
PJYARA(81)	Free-stream values of current density component J_y	(A/m^2)
PINF	Static pressure, local	(N/m^2)
RHO(43)	Mass density	(kg/m^3)
SF	Seed fraction	
SIGMA(43)	Scalar conductivity	(mho/m)
TAU(43)	Turbulent shear stress, τ	($kg/(ms^2)$)
TEMP(43)	Gas temperature	(^oK)
TEMPE(43)	Electron temperature	(^oK)
TW	Wall temperature	(^oK)
U(43)	Gas velocity	(m/s)
UARA(81)	Free-stream values of gas velocity	
XNE(43)	Electron number density	(m^{-3})
Y(43)	Distance from wall	(m)
YL	Boundary layer thickness δ_{995}	(m)

APPENDIX C
DEFINITION OF TERMS USED IN THE BOUNDARY LAYER SOLUTION

For the convenience of the reader, and because conflicting definitions are sometimes used in the literature, some of the important boundary layer parameters will be defined clearly in this Appendix. The definitions given here will correspond to the way these terms have been used in this study.

(1) Boundary layer thickness δ

As explained in Ref. 3, the boundary layer solution uses the normalized cross-coordinate ω defined by

$$\omega = \frac{S - S_I}{S_E - S_I} \tag{C1}$$

where S is the streamfunction and S_I and S_E its values on the wall and on the free-stream, respectively.

Eq. (C1) defines the correspondence between ω and the geometrical cross-coordinate y: Since $\partial S/\partial y = \rho u$, it follows that at each station x,

$$d\omega = \frac{\rho u}{S_E - S_I}\, dy \tag{C2}$$

or

$$y = (S_E - S_I) \int_o^\omega \frac{d\omega}{\rho u} \tag{C3}$$

We define as δ the value of y corresponding to $\omega = 1$, namely

$$\delta \equiv (S_E - S_I) \int_o^1 \frac{d\omega}{\rho u} \tag{C4}$$

The value of $S_E - S_I$ at each station x is found by integrating the entrainment rate $\dot{m}_E$ and the wall injection rate $\dot{m}_I$, since, by definition,

$$\frac{d}{dx}(S_E - S_I) = -(\dot{m}_E - \dot{m}_I) \tag{C5}$$

or

$$S_E - S_I = (S_E - S_I)_{x=0} - \int_o^x (\dot{m}_E - \dot{m}_I)\, dx \tag{C6}$$

The integrations indicated by Eqs. (C3), (C4), and (C6) are carried out numerically.

(2) Displacement thickness δ^* and momentum thickness θ

These are defined as usual, namely

$$\delta^* \equiv \int_o^\delta (\rho_\infty U_\infty - \rho u)/\rho_\infty U_\infty\, dy \tag{C7}$$

$$\theta \equiv \int_o^\delta \rho u(U_\infty - u)/\rho_\infty U_\infty^2\, dy \tag{C8}$$

It is clear from Eq. (C.2) that

$$S_E - S_I = \int_o^\delta \rho u\, dy \tag{C9}$$

and therefore the above definitions can be written in the form

$$\delta^* = \delta - (S_E - S_I)/\rho_\infty U_\infty \tag{C10}$$

$$\theta = \delta - \delta^* - \frac{1}{\rho_\infty U_\infty^2} \int_o^\delta \rho u^2\, dy$$

$$= (\delta - \delta^*)\left[1 - \int_o^1 (u/U_\infty)\, d\omega\right] \tag{C11}$$

These are the expressions used in this study.

(3) Skin friction coefficient c_f and heat transfer coefficient St

After the wall shear τ_w and the wall heat flux q_w are computed, we calculate c_f and St through the following definitions

$$c_f \equiv \tau_w/(\tfrac{1}{2}\rho_\infty U_\infty^2) \tag{C12}$$

$$St \equiv -q_w/\rho_\infty U_\infty (H_\infty - H_w) \qquad (C13)$$

where H is the total specific enthalpy $H = h + \frac{1}{2} u^2$.

UNCLASSIFIED

Security Classification

DOCUMENT CONTROL DATA - R & D

(Security classification of title, body of abstract and indexing annotation must be entered when the overall report is classified)

1. ORIGINATING ACTIVITY *(Corporate author)*
STD Research Corporation
Box 4127, Catalina Station
Pasadena, California 91106

2a. REPORT SECURITY CLASSIFICATION
UNCLASSIFIED

2b. GROUP
N/A

3. REPORT TITLE

CURRENT DISTRIBUTION IN CROSSED-FIELD ACCELERATORS (PART IV, PROJECT SUMMARY AND APPLICATION)

4. DESCRIPTIVE NOTES *(Type of report and inclusive dates)*
Final Report - 1 July 1969 to 30 September 1970

5. AUTHOR(S) *(First name, middle initial, last name)*

G. S. Argyropoulos and S. T. Demetriades

6. REPORT DATE
April 1971

7a. TOTAL NO. OF PAGES
70

7b. NO. OF REFS
15

8a. CONTRACT OR GRANT NO.
F40600-70-C-0001

b. PROJECT NO 8950

c. Program Element 62201F

d. Task 895012

9a. ORIGINATOR'S REPORT NUMBER(S)
AEDC-TR-71-91

9b. OTHER REPORT NO(S) *(Any other numbers that may be assigned this report)*
Research Report STD 70-6

10 DISTRIBUTION STATEMENT
Approved for public release; distribution unlimited.

11 SUPPLEMENTARY NOTES
Available in DDC

12. SPONSORING MILITARY ACTIVITY
Arnold Engineering Development Center, Air Force Systems Command, Arnold AF Station, Tenn. 37389

13. ABSTRACT Realistic analytical modeling of crossed-field accelerators is obtained by computing the development of turbulent magnetohydrodynamic boundary layers on the walls and the coupled two-dimensional distributions of current density, plasma properties, and fluid velocity, temperature and pressure over the entire channel. The analysis is based on methods developed in previous work by the authors, and considers the effects of electron nonequilibrium, thermal and concentration diffusion, suppression of turbulence by magnetic fields, finite reaction rates, and electron energy relaxation. Application to the Hirho channel gives excellent agreement with experimental results. It is shown that the reduction of the Hall field in Faraday channels is due to the fact that local axial current density is present over most of the flow, even when there is no net current leakage along the channel. The modeling is carried out by a well-documented computer program, of which a program listing, Fortran source deck, and explanation of input and output formats are provided. This work has demonstrated that realistic computations are necessary for the design of efficient magnetohydrodynamic channels.

DD FORM 1 NOV 65 1473

UNCLASSIFIED

Security Classification

14. KEY WORDS	LINK A		LINK B		LINK C	
	ROLE	WT	ROLE	WT	ROLE	WT
modeling						
J X B accelerators						
turbulent MHD boundary layers						
current distribution						
potential distribution						
plasma property distribution						
velocity profile						
shear stress profile						
gas tempeature profile						
electron number density profile						
electron temperature profile						
electron nonequilibrium						
thermal and concentration diffusion						
suppression of turbulence						
finite reaction rates						
electron energy relaxation						
multielectrode geometries						
magnetohydrodynamics						